Featuring work from the iMedication Lab of Professor Zhen Gu and Professor Yuqi Zhang, College of Pharmaceutical Sciences, Zhejiang University, China.

Microneedle-based transdermal detection and sensing devices

An overview of the recent works on microneedle-mediated detection and sensing systems, covering the principles, integration formats, and objective significance along with a wide range of physical or biochemical targets, as well as an insight into challenges and perspectives of the field.

As featured in:

ROYAL SOCIETY
OF **CHEMISTRY**

rsc.li/loc

Check for updates

Microneedle-based transdermal detection and sensing devices

Junxia Wang, [iD] [a] Ziyi Lu, [iD] [ab] Ruisi Cai,[a] Hanqi Zheng,[a] Jicheng Yu,[abcd] Yuqi Zhang*[ae] and Zhen Gu [iD] *[abcdf]

Microneedles have been expected for the construction of next-generation biosensors towards personalization, digitization, and intellectualization due to their metrics of minimal invasiveness, high integration, and favorable biocompatibility. Herein, an overview of state-of-the-art microneedle-based detection and sensing systems is presented. First, the designs of microneedle devices based on extraction mechanisms are concluded, corresponding to different geometries and materials of microneedles. Second, the targets of equipment-assisted microneedle detections are summarized, as well as the objective significance, revealing the current performance and potential scenarios of these microneedles. Third, the trend towards highly integrated sensors is elaborated by emphasizing the sensing principles (colorimetric, fluorometric and electronic manner). Finally, the key challenges to be tackled and the perspectives on future development are discussed.

[a] *Zhejiang Provincial Key Laboratory for Advanced Drug Delivery Systems, College of Pharmaceutical Sciences, Zhejiang University, Hangzhou, 310058, China. E-mail: yqzhang21@zju.edu.cn, guzhen@zju.edu.cn*
[b] *Department of General Surgery, Sir Run Run Shaw Hospital, School of Medicine, Zhejiang University, Hangzhou, 310016, China*
[c] *Jinhua Institute of Zhejiang University, Jinhua, 321299, China*
[d] *Liangzhu Laboratory, Zhejiang University Medical Center, Hangzhou, 311121, China*
[e] *Department of Burns and Wound Center, Second Affiliated Hospital, School of Medicine, Zhejiang University, Hangzhou, 310009, China*
[f] *MOE Key Laboratory of Macromolecular Synthesis and Functionalization, Department of Polymer Science and Engineering, Zhejiang University, Hangzhou, 310027, China*

1. Introduction

Usage of mobile devices such as sports watches and smart bracelets for monitoring vital signs has exponentially increased, becoming routine for tracing daily exercise as well as heart rate and sleep quality.[1] In addition to vital signs, a wearable device that could further indicate and monitor the physiological conditions inside the body is urgently demanded, such as blood glucose and lactate signals. However, many of these are usually associated with blood tests. Statistically, 20–50% of children, and 20–30% of adults, suffer from needle phobia, especially those patients who require frequent blood testing.[2] The desire for minimally

Junxia Wang received her bachelor's degree in Chemistry (2016) and PhD degree in Biological Chemistry (2021) from Xiamen University (advisor: Professor Zhi Zhu and Professor Chaoyong Yang). Currently, she is a postdoctoral researcher in Professor Zhen Gu's iMedication lab at Zhejiang University. Her research interest focuses on microneedle-based mRNA delivery, and microfluidics-based molecular evolution.

Junxia Wang

Yuqi Zhang is an Assistant Professor at the College of Pharmaceutical Sciences at Zhejiang University. Dr. Zhang received her B.S. degree in Chemistry from Nanjing University. In 2018, she obtained a Ph.D. from the Joint Department of Biomedical Engineering at the University of North Carolina at Chapel Hill and North Carolina State University. Dr. Zhang's group research interests focus on nano/microdrug delivery devices and biomaterials.

Yuqi Zhang

invasive biosensing devices has increased, posing challenges for the biosafety, patient compliance and multi-functionality of wearable devices.

Microneedles, a type of needle mostly shorter than 2 mm, have become an attractive minimally invasive transdermal approach. The original concept of microneedles was described in the 1970s. Along with the development of etching techniques, the first microneedle-structured array was reported by Hashmi et al. in 1995,[3] and subsequently, Henry et al. firstly applied them in the transdermal delivery of calcein AM.[4] The first microneedle-based sensing method, employing silicon microneedles in combination with a microcuvette for glucose level determination in blood, emerged in 2000.[5] In the 2010s, Gu and coworkers integrated a glucose-sensitive component and a drug release component into a microneedle array patch for closed-loop insulin delivery.[6,7] Since then, applications of microneedles have been investigated for more than two decades, involving biofluid sampling, instrument-coupled detecting, integrated sensing, and drug delivery.

As an attractive platform, microneedles offer the following advantages in sampling, detection, and sensing areas. Fine designed shapes of microneedles enable minimalized invasive insertion with high patient compliance. Diverse choices of materials and easy manufacturing allow high integration and flexible modification, providing opening scopes for biological sensing. The fabrication of microneedles could be cost-effective and mass-productive, offering vast possibilities for productization, marketization, and terminalization. To date, microneedle-based assays not only facilitate fitness adjustments, daily health management, and disease progression tracking, but also provide new insights into agricultural virus prevention, drug abuse control and food safety inspection.[8–12]

The majority of detection or sensing-aimed microneedles are still in the clinical trial stage. Only the TAP device,[13–15] a microneedle-based minimal blood collection device (~100 μL), has been approved by the FDA for use in hospitals, clinics, pharmacies, laboratories, and other settings. Taking diabetes monitoring as an example, TAP could be used to perform glycated hemoglobin testing, which is an indicator typically associated with blood glucose levels in diabetic people. In fact, microneedles are currently mostly commercialized in the field of cosmetics. Moreover, there are also several microneedles approved for transdermal injection and delivery of vaccines, insulin, or anesthetics, including Soluvia® (Becton-Dickinson Technologies),[16] Intanza® (Sanofi Pasteur),[17] MicronJet® (NanoPass Technologies),[18] etc.

In this review, we focus on state-of-the-art microneedle-based sampling, detection and sensing devices. First, the microanatomy of the skin and biofluids is introduced, and extraction mechanisms are concluded to guide the shape design and material optimization of microneedles. Second, the targets and significances of equipment-assisted microneedle detections are surveyed to reveal the current performance and potential scenarios of these microneedles, including physiological indicators, ions, small molecules, nucleic acids, proteins, cells and bacteria, as well as multiplex assays. Third, the trend towards highly integrated sensors is elaborated by emphasizing the inside sensing principles (colorimetric, fluorometric and electronic manner). Finally, the current challenges to be tackled and the perspectives on future development are also discussed to fulfil the great potential of this technology.

2. Design and fabrication of microneedle devices

Understanding the microanatomy of the skin is important for the design and fabrication of microneedle sensing devices. An ideal device must be capable of successfully penetrating the skin, reaching the targeted biofluid, and accomplishing sensitive detection. The fabrication methods and compositions of microneedles for blood sampling have been elaborately surveyed by Xue et al.[19] Thereby, in this section, we mainly focus on the design of microneedle devices in terms of the morphology and extraction mechanisms. The structural basis of skin along with the distributions and components of biofluids (e.g., blood, ISF) will also be discussed.

2.1 Skin and biofluids

Human skin consists of two layers, namely the epidermis (50–150 μm thick) and dermis (400–2400 μm thick). The outermost layer of the epidermis is the stratum corneum (10–20 μm thick), which consists of 15–20 layers of horny cells (fully keratinized keratinocytes). The horny cells are filled with keratin and surrounded by lipid-based intercellular matrix, forming a "brick-and-mortar" structure. The stratum

Zhen Gu

Zhen Gu is a Qiushi Distinguished Chair Professor and Dean of the College of Pharmaceutical Sciences at Zhejiang University. Dr. Gu received his B.S. degree in chemistry and M.S. degree in polymer chemistry and physics from Nanjing University. In 2010, he obtained his Ph.D. degree in chemical and biomolecular engineering at the University of California, Los Angeles (UCLA). Before he moved to Zhejiang University in 2020, he had been a Full Professor in the Department of Bioengineering at UCLA. His group focuses on controlled drug delivery, bio-inspired materials and nanobiotechnology, especially for cancer and diabetes treatment.

corneum is the stiffest part of the skin with an elastic modulus of 1–1000 MPa, depending on the skin source and hydration degree.[20–22] Underneath the stratum corneum is the variable epidermis, which is also an avascular region. The variable epidermis is less stiff compared to the stratum corneum, with an elastic modulus of around 10 MPa.[22] The innermost layer of the variable epidermis is the stratum basale. It consists of a single layer of keratinocytes, which continuously divide, keratinize, and move outward to form the other layers (stratum spinosum, stratum granulosum, stratum lucidum, and finally stratum corneum). The stratum basale is attached to a basement membrane, which separates the epidermis from the dermis. The dermis consists of a thin superficial papillary layer and a thick deep reticular layer, both being rich in capillaries, lymphatic vessels, free nerve endings and fibers. Unlike that of the epidermis, the elastic modulus of the dermis is only several tens of kPa.[23]

Blood tests have long been the gold standard for clinical diagnosis. The blood in the skin is mainly delivered by the capillaries in the dermis, which consists of two intercommunicating plexuses: the superficial plexus (300–600 μm depth) located at the junction of the papillary layer and reticular layer, and the deeper plexus (1300–1500 μm depth) situated at the dermal–subcutaneous junction.[24] Generated by blood transcapillary filtration, ISF is contained in all layers of the skin underneath the stratum corneum and accounts for 45% of the skin volume (blood only 5%).[25] There are three dominant pathways for the analyte exchange of ISF: transcellular for analytes around a few hundred Daltons or less and uncharged analytes like glucose; paracellular and transcytosis for larger and charged analytes like proteins.[26] Therefore, the ISF concentrations of electrolyte ions (e.g., Na^+, K^+), small molecules (e.g., glucose), and some diets (e.g., caffeine, alcohol) are comparable to the plasma concentrations.[27–31] However, some hormones like cortisol or antibiotics like penicillin and vancomycin are protein bound. Their concentrations in ISF are only equal to the free state concentrations in plasma, excluding the protein-bound ones.[32–34] Reported concentrations of common biological analytes in blood and ISF have been surveyed and are presented in Table 1. To make full contact with the capillary plexus, microneedles for blood extraction are generally longer than 1500 μm.[19,35,36] However, microneedles for ISF extraction could be as short as 100 μm,[37] and the needle length is usually less than 1500 μm to avoid blood drawing.

2.2 Microneedles for skin penetration

To penetrate the stratum corneum, the microneedle must have a sharp tip and a robust body to avoid bending or breaking. The morphology of a microneedle in a transdermal detection system can be classified as hollow, porous or solid. Generally, hollow microneedles are relatively brittle, and are composed of materials with high mechanical strength. Therefore, long hollow microneedles (>1500 μm long) are usually a single stainless-steel needle,[35,36] but short hollow microneedles can be made of various materials (titanium,[38] Si,[39] glass,[40] polymers[41]) and can be arranged into an array. Clogging is another major concern during biofluid extraction, especially for microneedles with straight sidewalls. Snake-fang-like hollow microneedles can mitigate cell-cutting and avoid clogging issues during insertion, due to the tapered sidewalls and the pore on the edges.[39,42] Different from the single-channel hollow microneedles, porous microneedles are featured with internally connected capillary channels. Limited by the stringent conditions in ceramic or metal manufacturing (e.g., processing temperature >1000 °C),[43] porous microneedles are usually made of polymers. However, polymer porous microneedles are also physically brittle. One attempt to increase mechanical strength is combining porous structures with solid microneedle substrates. Puttaswamy et al. coated porous PLGA on the surface of malt sugar microneedles.[44] Core–shell microneedles could sustain ten times the force required to penetrate the skin.[45] Similarly, Samant et al. fixed a porous filter paper between two flat stainless-steel microneedles to ensure efficient penetration.[46] Hydrogels, rigid in the dry state, and swellable into porous structures after water absorption, enable both effective skin penetration and biofluid extraction for microneedles. He et al. constructed a microneedle patch made of a polyvinyl alcohol (PVA) hydrogel with 20% chitosan (CS), achieving a 75% porosity with an average diameter of around 20 μm.[47] After insertion to rabbit skin, no needle tip was broken although some were slightly blunted. Moreover, hydrogels

Table 1 ISF compositions and the corresponding physiological concentrations

Analytes	Molecular weight (Da)	Blood/plasma	ISF	Ref.
Na^+	23.0	~136 mM	Similar	27
K^+	39.1	~3.97 mM	Similar	27
Glucose	180.2	1.6–28.4 mM	Similar	28
Lactate	90.1	6.9–24.9 mg dL^{-1}	20.6–56.6 mg dL^{-1}	29
Caffeine	194.2	Can reach several tens of μM	Similar	31
Alcohol	46.1	Can reach several tens of mM	Similar to a breathalyzer outcome (a direct estimation of blood alcohol content)	30
Cortisol	362.5	Hundreds of nanomolars (~90% protein bound)	Similar to unbound in plasma	32
Penicillin G	334.4	~60% protein bound	Similar to unbound in plasma	33
Vancomycin	1449.3	~55% protein bound	Similar to unbound in plasma	34

can be coated around solid microneedles to obtain better mechanical strength.[48,49] Solid microneedles are most likely to penetrate the skin for long-term monitoring.[30,50] Zheng *et al.* designed field effect transistor electrode-combined solid polystyrene microneedles.[50] This sodium biosensor platform was tested on healthy individuals and achieved excellent on-body monitoring for several hours.
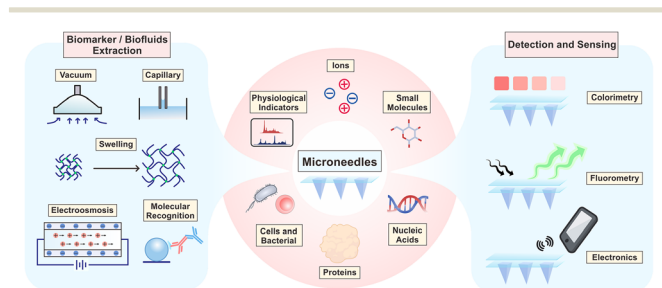
2.3 Microneedles for biomarker extraction

For biofluid extraction, mainly five kinds of mechanisms are involved (Fig. 1). First, a vacuum drives the biofluids to flow through pressure differences between the skin and the microneedles. The vacuum-based extraction could be initiated with a vacuum actuator, which is pre-stored[35] or press-generated,[36] and is usually combined with a long stainless-steel hollow microneedle. Besides direct microneedle extraction, a vacuum could also propel the aspiration of blood or ISF through micropores punched by a solid microneedle array.[15,31] To reduce pain and increase penetration efficiency, these microneedles are usually 2D-structured and made of stainless-steel. Interestingly, Miller *et al.* described a vacuum-free hollow microneedle with a cylinder concentric substrate for pressure-driven ISF extraction. The unique opening design could generate a local pressure at tissues surrounding the insertion point. Consequently, about 1.5 μL of ISF was transported into a single microneedle without the need of additional vacuum.[40] Second, capillary force could push the blood or ISF flow along lyophilic solid surfaces (*e.g.*, in the narrow channel in hollow microneedles) based on the biased solid–liquid interfacial interaction. However, the inner diameter of stainless-steel hollow microneedles is often too large (>60 μm) to provide sufficient capillary force. Therefore, Si is mainly used to prepare ultra-fine hollow microneedles.[37,42] Strambini *et al.* fabricated a silicon-based microneedle patch *via* an etching–oxidation process, achieving an inner diameter of 4 μm and a needle density of 1×10^6 needles per cm².[37] The high-density microchannels with a comparable diameter to porous microneedles provided enough capillary force and reached an ISF extraction rate of 1 μL s⁻¹. Moreover, capillaries in a porous structure (typically made of

PLGA with a porogen) can automatically absorb liquids *via* capillary force. As blood passes through the porous structure, blood cells are trapped, leaving only the plasma.[44] Third, swellable hydrogels can extract ISF without additional forces. Once contact is made with ISF, the hydrogel surface will be surrounded by solvent molecules and start expanding, allowing for further molecule transportation into the hydrogel network. Among them, cross-linked hydrogels made of methacrylated hyaluronic acid or gelatin showed the most rapid absorption and the largest swelling ratio, making them ideal for biofluid extraction (Fig. 2A).[34,51] The extraction ability is highly dependent on the concentration of monomers and the polymerization time.[34] Fourth, electroosmosis on microneedles has been used for ISF extraction.[52,53] Electroosmosis refers to the convective solvent flow when an electric field is applied across a solution near a charged surface. The electroosmosis flow direction and rate could be controlled by modifying different charged groups on the porous surface (*e.g.*, sulfonic groups, quaternary amine groups).[52] Fifth, specific interaction by antibody or aptamer recognition has also been applied in blood or ISF extraction using microneedles (Fig. 2B). Generally, solid or core–shell microneedles are coated with a high density of recognition molecules, and a porous surface can further increase the contact area.[54,55] Wang *et al.* introduced antibody-coated microneedles to capture desired antigens to realize an ultrasensitive assay.[56] A similar strategy was applied for cell capture. Mandal *et al.* applied adjuvants and specific antigens to attract the surrounding immune cells into microneedles.[48]

3. Equipment-assisted microneedle sensors

With the increased demand for point-of-care testing, microneedles with high patient compliance have become an ideal option for the construction of wearable sensors. Microneedle-assisted detection or sensing systems are

Fig. 1 Overview of microneedle-based transdermal detection and sensing devices, including biomarker/biofluid extraction strategies (left), different targets (middle), and detection and sensing principles (right).
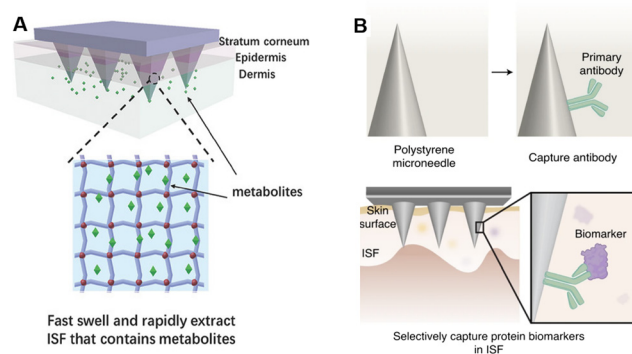
Fig. 2 Schematic illustrations of different extraction mechanisms of (A) swelling-based extraction. Reproduced with permission.[51] Copyright 2017, Wiley-VCH Verlag. (B) Antibody-based extraction. Reproduced with permission.[56] Copyright 2021, Springer Nature Publishing.

featured with rapid responses, wide working ranges, and low detection limits. In some recent cases, microneedles enabled continuous monitoring, multiplex analysis, and even intelligent medication.[57] So far, targets of equipment-assisted microneedles have covered physiological indicators, ions, small molecules (glucose, lactate, drugs, and others), nucleic acids, proteins, cells and bacteria, in a single or multiplex analysis manner (Fig. 1). Some recent representative studies in this section are summarized in Table 2, indicating the targets, compositions, working ranges, time consumptions, and the assistant equipment. In this section, we would emphasize the significance and state-of-the-art microneedle assays according to the classification of targets. The validation models (*in vitro*, *ex vivo*, *in vivo*, and human volunteers) and clinical trials are also included.

3.1 Physiological indicators

Physiological indicators mainly include mechanical forces, electromyograms (EMGs), electrocardiograms (ECGs), electroencephalograms (EEGs), *etc.*

Mechanical forces are essential in the interaction of cells with their surrounding extracellular matrix (ECM). To evaluate interactions inside cells, Tan *et al.* proposed a PDMS-based elastomeric microneedle array. Cells could attach to multiple posts, resulting in deflection in needles, and the degree of deflection observed by confocal microscopy could directly indicate the traction of the subcellular force distributions (Fig. 3A).[58] Besides, miniaturized force sensors could offer the surgeon imperceptible force information, improving the accuracy and safety of retinal microsurgery. To assist retinal vein cannulation practice, Gonenc *et al.* attached two fiber Bragg grating (FBG) sensors on one hollow stainless-steel microneedle. Tests on fertilized eggs showed a 100% success in cannulation, demonstrating the feedback sensing of the microneedle sensors.[59] Similarly, while previous studies focused on 2D mechanical monitoring, Zhang *et al.* took it further into 3D force sensing, by increasing the number of optical fibers into three. Benefiting from this novel FBG configuration, the detection sensitivity was also improved.[60]

Biosignals like EMGs, ECGs, and EEGs are all tightly related to physiological status. Particularly, at-home surveillance devices to measure these biosignals are expected to be wearable, miniaturized, highly biocompatible, and stable to meet the needs of long duration monitoring. For the sake of improving biocompatibility, the main body of these MNs is commonly made of titanium, polyimide, and silicon.[61]

EMGs provide the opportunity to evaluate and record the electrical activity generated by skeletal muscles. Kim *et al.* proposed a curved microneedle array integrated with a band. The EMG signals before and after 20 min of stair climbing exercise were recorded and compared with those of commercial electrodes, with the microneedles exhibiting improved sweating-tolerance.[62] Guvanasen *et al.* designed

stretchable PDMS microneedles to cover and monitor the lateral gastrocnemius muscle in felines. The microneedles could bear repeated stretching of up to 40% tensile strain.[63]

ECGs can be sensed with microneedle electrodes by measuring minor electrical changes in the skin, which come from the depolarization and repolarization of the heart muscle during heartbeats. Wang *et al.* fabricated a PDMS microneedle array and coated it with a layer of Ti and a layer of Au, achieving a smaller impedance and higher signal quality during ECG monitoring.[64] Long-term monitoring as long as 48 h has been achieved, as well as human volunteer testings.[65]

EEGs reflect voltage fluctuations caused by ionic currents in neurons, and are commonly used to diagnose epilepsy, sleep disorders, coma, encephalopathy, and even brain death. Microneedles enable the direct collection of an EEG, without the need of hair cutting or gel smearing, providing a user-friendly approach for patients needing long-term monitoring. Wang *et al.* fabricated a MEMS-based pyramid microneedle array for long-time EEG measurement. The impedance of the microneedle electrode was found to be much more stable than that of a standard electrode within a 5 h monitoring.[66]

3.2 Ions

Electrolyte imbalances (hyperkalemia, hypernatremia, hypokalemia, and hyponatremia) lead to certain physical disorders, which in turn bring a range of clinical symptoms such as cardiac arrhythmias, muscle spasms, and even death. To determine the concentrations of physiological K^+ in the presence of interfering ions, Miller *et al.* reported a hollow microneedle characterized by ion selective electrodes (ISEs).[67] Through ISEs, the dominant ionic activity is selectively converted into potential differences, the value of which is related to the logarithm of the ionic activity on the principle of the Ernst equation.[68] Moreover, Li *et al.* realized the continuous sensing of K^+ and Na^+ in a chicken skin model. The improved sensor could continuously monitor for over 30 days in an artificial ISF with high accuracy.[69]

Acid/base disorders are closely associated with renal failure, ischemia, multiple sclerosis and psychiatric disorders. Therefore, monitoring the dynamics of pH in the body is also of great significance for health monitoring and disease progression indication.[70] To realize pH sensing, Lee *et al.* fabricated a conformable microneedle array with epoxy siloxane and polydimethylsiloxane. Polyaniline, whose conductivity is strongly influenced by pH, was coated on microneedles, realizing sensitive and persistent skin pH monitoring in a peripheral artery disease (PAD) mouse model.[71] Mani *et al.* proposed an electrode-based microneedle to achieve label-free and real-time pH sensing. The *in vivo* performance of this microneedle was demonstrated in mouse cerebrospinal fluid (CSF) and bladders, indicating a wide range of potential clinical applications.[72] Moreover, specific molecules binding with H^+ or responding to various pH levels would improve the

Table 2 Representatives of recent microneedle-assisted detection systems

Targets	Microneedle compositions	Detection ranges	Time consumptions/continuous sensing	Related equipment	Ref.
Subcellular mechanical force	PDMS-MNs coated with fibronectin or collagen IV	>12 nN	—	Confocal microscopy	58
Two-degrees of freedom (DOF) force	Stainless steel-MNs with silica epoxy resin optical fibers, and a nitinol tube	0.25–15 mN	—	Fiber Bragg grating (FBG) interrogator	59
Three-degrees of freedom (DOF) force	Stainless steel-MNs with silica epoxy resin optical fibers, and a nitinol tube	>0.124 mN for the X/Y direction, >0.74 mN for the Z direction	—	Fiber Bragg grating (FBG) interrogator	60
K^+	Eshell 300-MNs with PMMA microfluidic channels	10^{-5}–10^{-2} M	20 s for stabilization	Potentiostat	67
K^+, Na^+	A 26-gauge hypodermic needle assembled with a PDMS substrate, and electrodes	5–200 mM for NaCl, and 1–15 mM for KCl	<100 s	Potentiostat	69
pH	Epoxy siloxane-MNs with a PDMS substrate	pH = 3–7	Continuously sensing for 5 h	Electrochemical analyzer	71
pH	Stainless-steel acupuncture needles	pH = 4–8	5 min for a single response, continuously sensing for >40 min	Micro Raman spectrometer	74
pH	(NOA) 65-MNs	pH = 5–9	—	Microscopy with extra-long working distance (ELWD) objectives	73
Lactate	PC–MNs with Au electrodes and nanocarbons	10–200 μM	—	Potentiostat	77
Lactate	Pt–MNs with functional electrodes	0.375–12 mM	—	Potentiostat	78
β-Hydroxybutyrate, glucose	Carbon paste-filled hollow MNs with electrodes	0.05–12 mM for β-hydroxybutyrate, 1–10 mM for glucose	Continuously sensing for 4 h	Potentiostat	99
Alcohol	Stainless steel-MNs with a Pt wire multilayer transducer	5–80 mM	Continuously sensing for 100 min with 10 min intervals	Potentiostat	93
H_2O_2	Steel-MNs coated with GO/H_2PtCl_6	0.4–20 mM	5 min	Electrochemical workstation	95
Urea	c-GelMA-MNs	—	—	Commercial urea kit	97
Vancomycin	Au-coated Ni–MNs with optofluidics	0.1–72.6 μM	10 min	—	87
Morphine and fentanyl	Hollow MNs with working electrodes and carbon paste transducers	20–140 μM for morphine, 10–200 μM for fentanyl	1 min for a single time of response, continuously sensing for 3 h	Potentiostat	11
Fentanyl	Pt–MNs with electrodes modified by graphene ink	27.8–160 μM	—	Potentiostat	89
Apomorphine	Resin-MNs with electrodes	20–100 μM	Continuous sensing for 2 h with 10-min intervals	Potentiostat	90
Levodopa	Resin-MNs with electrodes	5–300 μM	Continuous sensing for 2 h with 10 min intervals	Potentiostat	91
DNA of *Phytophthora infestans*	PVA-MNs	1.2 pg μL^{-1} to 12 ng μL^{-1}	1 h	Thermal cycler	10
DNA of Epstein–Barr virus	PMVE/MA-MNs	1.5×10^4–5.0×10^6 copies per μL	15 min	Microfluidic biosensors with a potentiostat	102
DNA of Epstein–Barr virus	PMVE/MA-MNs with printed nanotubes	5.0–1.0×10^4 copies per μL	10 min	Potentiostat and electrochemical microfluidic biosensor	103
DNA of Epstein–Barr virus, sepsis-associated cfDNA, and kidney transplantation-associated cfDNA	PMVE/MA-MNs with printed nanotubes	3×10^{-14}–3×10^{-11} M	Continuous sensing for 8 days	Electrochemical workstation	104
DNA of the allergized domain in milk and shrimps	PVA-MNs	0.00003 ppm for milk DNA, and 0.00005 ppm for shrimp DNA	<1 h	Thermal cycler	105

Table 2 (continued)

Targets	Microneedle compositions	Detection ranges	Time consumptions/continuous sensing	Related equipment	Ref.
miRNA	PLLA-MNs coated with alginate and peptide nucleic acid	6–500 nM	<0.5 h	Fluorescence scanner	49
miRNA	GO-GelMA-MNs	500 pM–500 nM	1 h	Confocal microscope	116
Myoglobin and troponin	Au–MNs with electrodes	100–1000 ppb	—	Potentiostat	108
Epidermal growth factor receptor 2	Si–MNs with Au electrodes	50–250 ng mL^{-1}	<1 h	Potentiostat	9
IL-8	Au–MNs embedded with microwells	62 pg mL^{-1} to 538.6 ng mL^{-1}	<20 min	Potentiostat	112
Cocaine antibody, interleukin 6, and periostin	PS-MNs with Fe$_3$O$_4$ nanoparticles in the substrate	0.33 pg mL^{-1} –2.5 ng mL^{-1} for cocaine antibody, n.s. for interleukin 6 and periostin	5 h	Fluorescence imager	56
E. coli	TMA/CAA/HEMA-MNs with Au-nanopopcorns	1.43×10^2 –2.4×10^6 cfu g^{-f}	<10 min	Raman spectrometer	113
Tissue-resident memory T cells	PLLA-MNs coated with alginate and sucrose	—	24 h	Flow cytometry	114
TNF-α, IL-1β, and IL-6	PEGDA/PEG/ HMPP-MNs coated with photonic crystals	10–500 ng mL^{-1} for TNF-α, IL-1β, and IL-6	<3 h	Spectrometer and luminoscope	115
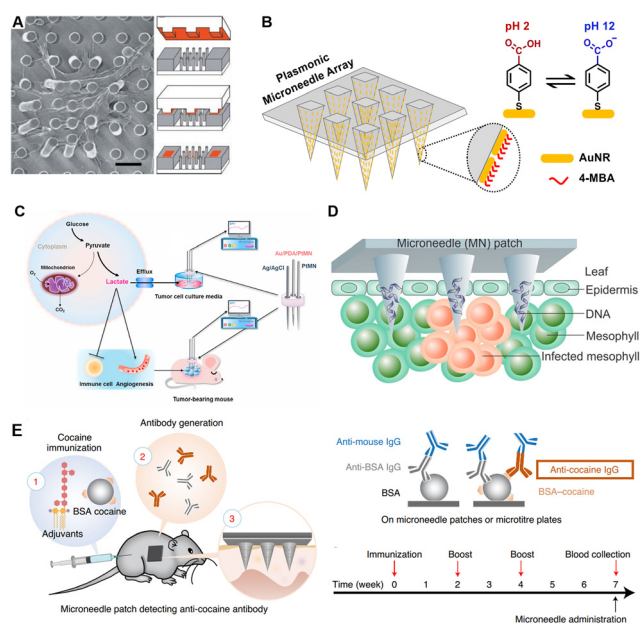
Fig. 3 Schematic illustrations of microneedles for detection of different targets. (A) Representative SEM images of cells attached to a microneedle array for single-cell force sensing. Reproduced with permission.[58] Copyright 2003, National Academy of Sciences. (B) Plasmonic microneedles coated with gold nanorods functionalized with pH-sensing molecules. Reproduced with permission.[73] Copyright 2019, American Chemical Society. (C) Electrochemical sensing platform for quantitative detection of lactate which was correlated with tumor progression. Reproduced with permission.[78] Copyright 2021, Elsevier. (D) Rapid extraction of plant DNA using swelling microneedles. Reproduced with permission.[10] Copyright 2019, American Chemical Society. (E) Minimally invasive detection of cocaine-specific antibodies in an immunized mouse model after microneedle extraction. Reproduced with permission.[56] Copyright 2021, Springer Nature Publishing. Copyright 2020, American Chemical Society.

specificity of microneedle analysis. Park *et al.* reported an *in situ* sensing plasmonic microneedle array that could work in the human skin, functionalized with pH-responsive 4-mercaptobenzoic acid-coated nanorods (Fig. 3B).[73] Besides conventional structures, acupuncture-derived microneedles have also been applied in pH sensing. Pan *et al.* etched two groves on one acupuncture needle, loaded with redox-responsive and pH-responsive SERS probes, respectively. In muscles, the redox and pH could be detected by this acupuncture-derived microneedle within 5 min.[74] Besides healthcare, applications of microneedles have been extended to food safety control. Li *et al.* utilized the above acupuncture-derived microneedle to detect the redox and acid states of peels, bananas, and strawberries, to avoid food exposed to the air.[75]

3.3 Small molecules

In addition to ions, small molecules (such as lactate, glucose, and drugs) are also highly mobile between the ISF and blood. Many analytes share the same concentration in ISF and blood, with a few exceptions (*e.g.*, lactate). *In situ* monitoring of small molecules has always been a mutual interest in the healthcare field. The physiological significance differs from one small molecule to another. In this section, we present the significance of detections of these small molecules, classified as lactate, glucose, drugs and others, while the corresponding sensing principles and validation models are also covered.

Lactate. Lactate is produced through the anaerobic glycolytic metabolic path, especially after exercise. Insufficient degradation of lactic acid causes muscle cramps, and the rapid rise of blood lactate levels during shock even

leads to coma. Real-time sensing of lactate is of great significance in sports medication. Recently, Ming *et al.* has published the first in-human data of the dynamic determination of lactate levels using microneedles. They found good tolerance and good agreement among volunteers in the phase I clinical study.[76] Lactate oxidase (LOX), the endogenous specialized enzyme for lactate oxidization, is the most frequently used lactate recognition element. Based on LOX catalysis, Bollella *et al.* fabricated gold microneedles with nanocarbons to realize real-time lactate monitoring in artificial interstitial fluid and human serum.[77]

Besides sports medicine, lactate is also a tumor biomarker. Cancer cells increase glucose consumption through glycolysis, while continuously pumping out lactate. This process promotes angiogenesis and immune escape. Thereby, the level of lactate is also an indicator of tumor stage, metastasis, and survival. Li *et al.* produced a lactate-sensing microneedle array and successfully recorded the lactate levels in tumor-bearing mice. The signal intensity was found to be associated with tumor burden and progression (Fig. 3C).[78]

Glucose. Microneedles for glucose sensing have been extensively exploited. There are many reviews devoted to surveying the histories of, progress in, and state-of-the-art systems for glucose monitoring on microneedles.[79–81] In this section, we mainly focused on recently published representative studies on fully-integrated microneedle-based glucose sensing.

According to the International Diabetes Federation, about 537 million adults and 1.2 million children and adolescents suffer from diabetes.[82] Hypoglycemia could lead to convulsions or coma, while chronic hyperglycemia causes eye and kidney injury. Long term monitoring of blood glucose levels is of substantial significance for diabetes management. For instance, for each additional day of sensor application per week, the glycated hemoglobin levels could be cut by an average of 0.15%.[83] However, the invasive and painful application of these devices limits patient compliance. More recently, glucose sensing devices are heading towards integration, digitalization, and wearability. Tehhrani *et al.* proposed a fully-integrated wearable microneedle sensor with a wireless transportation function for dual biomarker detection (lactate and glucose, or alcohol and glucose). This wearable device has been verified in volunteers performing common daily activities with robust analytical performances.[84] Moreover, Li *et al.* developed a wearable system to realize closed-loop treatment through sequential glucose sensing, signal transportation, and intelligent drug release. With incorporation with reversible iontophoresis (RI) microneedles and a flexible printed circuit board (PCB) controller, this device exhibited accurate tracking of glucose fluctuations and responsive release of enclosed insulin, successfully regulating the blood glucose levels in a diabetic rat model.[53] Besides, to overcome the low-throughput limitation of RI-based sensors, Cheng *et al.* constructed a fully-integrated touch-actuated glucose microneedle sensor,

achieving a 160% enhancement in extraction throughputs.[85] In addition, the combination of microneedles and stretchable soft electronic sensors could further improve a diabetic patient's compliance. Lee *et al.* applied a graphene–Au hybrid sensor with improved electrochemical activities in the construction of a wearable microneedle patch, which could monitor glucose levels in ISF and offer feedback therapeutics accordingly. The sweat-based sensing of glucose and pH was demonstrated in diabetic mouse models and two human volunteers.[86]

Drugs. There are strong correlations between ISF and blood levels of many drugs, including antibiotics, chemotherapy drugs, neurodegenerative disease drugs, and psychotropic drugs. Thereby, microneedles with high patient compliance could expand the toolbox of therapeutic drug monitoring (TDM).

Vancomycin (VAN), a specific antibiotic against Gram-positive bacteria, is the last choice for the treatment of methicillin-resistant *Staphylococcus aureus* infection.[87] However, excess VAN in circulating biofluids would lead to nephrotoxicity (renal failure) and ototoxicity (irreversible deafness). To monitor the VAN levels, Ranamukhaarachchi *et al.* developed an optofluidics-integrated hollow microneedle and analysed VAN levels through a competitive binding assay. Only sub-nanolitre volumes ($\sim$1 nL) of ISF were required to reach a wide working range.[87] Furthermore, Rawson *et al.* have reported the first in-human study of real-time electric monitoring of phenoxymethylpenicillin using microneedles. This evaluation has shown that the pharmacokinetics obtained by microneedle analysis and microdialysis were highly similar, and the area under the concentration (AUC)–time curve of the drug in ISF is similar to that in serum.[88]

For abuse management of addictive drugs such as opioids (OPs), a cost-effective and rapidly responsive sensing platform could be availed for drug control. Mishra *et al.* provided a wearable electronic microneedle device for the simultaneous and continuous monitoring of fentanyl and OP nerve agents. In a skin-mimicking gel model, screening for morphine and fentanyl has been demonstrated.[11] Moreover, Joshi *et al.* proposed an interference-free fentanyl detecting assay using microneedles, the sensing performance of which was verified in diluted serum.[89] Similarly, *in situ* monitoring of apomorphine[90] and levodopa[91] has also been validated in microneedles, providing attractive tools for drug abuse control.

Others. Alcohol abuse can lead to fetal alcohol spectrum disorders, cancers, cardiovascular diseases, liver cirrhosis, multiple psychiatric disorders, and pancreatitis.[92] Development of *in situ* alcohol testing reflects growing concern in personal health and road safety. Mohan *et al.* reported an enzyme-based microneedle sensor for continuous alcohol monitoring. The continuous analysis was tested on *ex vivo* mouse skins for 100 min, revealing the feasibility of a minimally invasive alcohol monitoring platform.[93]

Hydrogen peroxide (H_2O_2), a by-product of reactive oxygen metabolism and a hub for the interconversion of reactive oxygen species, is the most common reactive oxygen molecule in living organisms. H_2O_2 is closely related to apoptosis and cell proliferation, and the related signalling pathways are associated with asthma, inflammatory arthritis, atherosclerosis, neurodegenerative diseases, *etc.*[94] Jin *et al.* proposed a microneedle-based electrochemical biosensor, and achieved *in situ* and real-time sensing on pig skin and living mice. This work demonstrated a promising platform for highly sensitive H_2O_2 sensing, in a minimally invasive manner.[95]

Urea and uric acid are metabolites of proteins, and are excreted almost exclusively by the kidneys. The urea or uric acid level is clinically significant in assessing kidney function and monitoring kidney diseases.[96] To determine urea and indicate renal complaints, Fonseca *et al.* described a swelling microneedle platform for *ex vivo* extraction of urea. The subsequent urea detection was conducted with a commercial kit.[97] Moreover, He *et al.* reported a microneedle-based colorimetric tattoo sensor, whose colors changed with pH, glucose, uric acid, and temperature levels in four separated detection areas, realizing the simultaneous detection of the four targets *ex vivo*.[98]

Similarly, ketone body monitoring was also realized using microneedles. Since ketone body accumulation leads to hyperglycaemia and metabolic acidosis, complications of diabetic ketoacidosis often happen to diabetic patients, with potentially fatal consequences. Therefore, monitoring both blood glucose and ketone bodies is greatly needed for diabetic patients. Teymourian *et al.* proposed a real-time monitoring microneedle patch for the continuous detection of ketone bodies and glucose, by measuring β-hydroxybutyrate (a common ketoacidosis biomarker) through β-hydroxybutyrate dehydrogenase.[99]

3.4 Nucleic acids

Nucleic acids, including DNA, mRNA, and miRNA, play vital roles in genetic information storage and transition, and epigenetic regulation. As biomarkers, nucleic acid analysis has been widely used in the fields of viral or bacterial detection, individualized treatment customization, and social screening for epidemic and infectious diseases.

Plant diseases could bring a severe impact on agricultural productivity, while pathogen-induced poor harvest is a widespread issue. In terms of the in-field diagnosis of plant diseases, Paul *et al.* fabricated a swelling microneedle patch that could extract pathogen DNA (*Phytophthora infestans*) from field-infected tomato leaves. After extraction, conventional PCR was carried out to quantify the specific DNA fragment (Fig. 3D).[10] In order to expand application scenarios, they have also improved this device with an isothermal nucleic acid amplification approach and integrated it with a cellphone-based fluorescence analyzer.[100]

The Epstein–Barr virus (EBV), a DNA virus of the herpesvirus family, is the pathogen of infectious mononucleosis. EBV is closely associated with the development of nasopharyngeal carcinoma and childhood lymphoma, and has been classified as one of the potentially cancer-causing viruses.[101] Rapid sensing of EBV could facilitate the management of individual antiviral therapy. Yang *et al.* designed microneedles coated with specific oligonucleotides that could respond to EBV genome fragments, which were then sensed with an electrochemical microfluidic platform.[102] Furthermore, they combined this device with a reverse iontophoresis approach to realize a wearable EBV-sensing microneedle patch with improved DNA capture. This device could detect EBV DNA from tumor-bearing immunodeficient mice, and the limit of detection was lowered into several copies per μL *in vitro*, showing great progress for a wearable electronic healthcare device.[103] Recently, clustered regularly interspaced short palindromic repeats (CRISPR) technology has also been integrated into microneedle devices for analysis of nucleic acids. Yang *et al.* demonstrated a CRISPR-activated wearable system consisting of a flexible PDMS substrate, a pair of printed carbon nanotubes, and a three-electrode microneedle prototype functionalized with Cas9/sgRNA.[104] The wearable system achieved real-time monitoring of viruses, sepsis, and cell-free DNA with 60% fetal bovine serum interference. The *in vivo* studies proved its satisfying stability of over 10 days.[104]

On account of a large number of allergy sufferers, a rapid screening platform for allergens is indispensable for individualized daily healthcare. Li *et al.* reported a swelling microneedle array to screen the DNA of specific allergy sources (milk, shrimp) in foods, providing a promising daily health control candidate for allergic people.[105]

MicroRNA, a class of short noncoding RNAs (commonly 19–25 nucleotides), also holds wide potential to become an individual biomarker or in combinations. Sulaiman *et al.* proposed a hydrogel microneedle patch functionalized with peptide nucleic acid (PNA). The specific miRNA could bind with the conjugated PNA through base pairing, and was subsequently stained by DNA dye, enabling *in vivo* fluorescence detection of specific miRNAs in a psoriatic mouse model.[49]

3.5 Proteins

Proteins are the major conductor of life activities. The conformation, modification, and quantity of proteins could be affected by diseases, responses, and body recovery. As one of the broadest spectra of biomarkers, proteins have been the preferred target for terminal diagnostic testing.[106] Sensing of protein biomarkers, cytokines, and antibodies has been demonstrated on microneedles.

Myoglobin and troponin are the mostly used biomarkers of myocardial damage, which fall off from myocardial fibers during cell injury and then enter the biofluid circulation.[107] Miller *et al.* described a hollow microneedle array containing

electrodes for myoglobin and troponin detection. Although not fully integrated, this manuscript offered a proof-of-concept demonstration of on-needle detection of protein biomarkers.[108] Cystatin C, a protein marker reflecting the glomerular filtration rate, is an important indicator for the diagnosis of chronic kidney disease, and the prognosis of cardiovascular diseases.[109] Puttaswamy et al. provided a lab-on-a-microneedle device for localized surface plasmon resonance (LSPR) of cystatin C in buffer and blood samples.[44] Similarly, Dervisevic et al. proposed an electrochemistry microneedle sensor, enabling the quantitation of a breast cancer biomarker (epidermal growth factor receptor 2) in skin mimicking gels.[9] Chen et al. proposed a semi-localization microneedle system for detection of the carcinoma embryonic antigen in mice models and human volunteers bearing breast tumor.[110]

Cytokines, mostly secreted by immune cells, are a type of special small proteins with humoral regulating activities. Along with the expanded clinical immunotherapy, a cytokine-monitoring device could bring insight into subtle changes in the immune system, therefore guiding adaptive clinical treatments.[111] Song et al. proposed a microneedle and microwell-based impedance sensor against human interleukin 8 (IL-8). This microneedle in real-time monitored the IL-8 levels in a mouse model that endogenously expressed IL-8, and the results were comparable to those measured by the ELISA gold standard approach.[112]

Endogenous antibody detection is of particular interest for indication of vaccination efficacies and disease prognosis, and, in some cases, the epidemiological investigation of infectious diseases. Wang et al. proposed an immune sandwich-based microneedle array for ultrasensitive in situ detection of antibodies and cytokines. For the proof-of-concept demonstration, IL-6, periostin and cocaine antibody detection was realized in mice models with high biocompatibility, low detection limitation, and good reproducibility (Fig. 3E).[56]

3.6 Cells and bacteria

Microbial contamination is a severe global issue in public health. A non-invasive, rapid and accessible bacteria screening device would greatly aid in food safety control. Wang et al. described a zwitterionic microneedle array that could extract *E. coli* from mutton in 3 min, detect *E. coli* through SERS nanoparticles, and finally inactivate the bacteria through photothermal conversion.[113] Moreover, Kim et al. designed a bacteria-sensing microneedle that could punch commercial food packages, enabling downstream adaption at home. This microneedle could harvest fluids from inside the food through a capillary, and present them on two colorimetric bio-ink patterns, thus indicating contamination and spoilage through detection of *E. coli* and pH, respectively.[12]

Unlike those of bacteria, extraction and detection of cells using microneedles face practical issues. Most of cells that could be reached by microneedles are keratinocytes, whereas

the cells involved in conventional blood tests cannot cross the capillary clusters, and therefore are not available for microneedles. However, there are certain immune cells that prefer to remain in peripheral tissues like skin, rather than circulate in the bloodstream, such as tissue-resident macrophages, natural killer (NK) cells, NK T cells, B cells, and memory T cells. Mandal et al. presented a strategy to monitor the tissue-resident memory T cells (T_{RM} cells) in skin using microneedles. The T_{RM} cells were traced for months in the inoculated mouse, and the sampling from human skin explants was also demonstrated.[114]

3.7 Multiplex detections

Due to the easy integration virtue of microneedles, multiplex detections have always been demonstrated and innovated. Based on the decoding principle of multiple signals, these can be divided into color- and space-differentiated multiplex detections. Color-based multi-signal differentiation is a user-friendly option, but introduction of colorimetric agents of different colors could be technical. Thereby, different principles for introducing multiple colors are described below. Inspired by the wide color coverage of photonic crystals (PhCs), Zhang et al. loaded PhC barcodes into the tip of microneedles to encode and detect three cytokines (TNF-α, IL-1β, and IL-6) in a sepsis mouse model, which could be read and decoded with a spectrometer and a luminoscope (Fig. 4A).[115] Spatial isolation is also an ideal method to distinguish different signal sources. He et al. fabricated four spatially-isolated patterns on one microneedle array, enabling concurrent sensing of pH, glucose, uric acid, and temperature (Fig. 4B).[98] Meanwhile, due to the independent electrode fabrication, spatial separation was easier to achieve in the electrode-functionalized microneedles. For example,
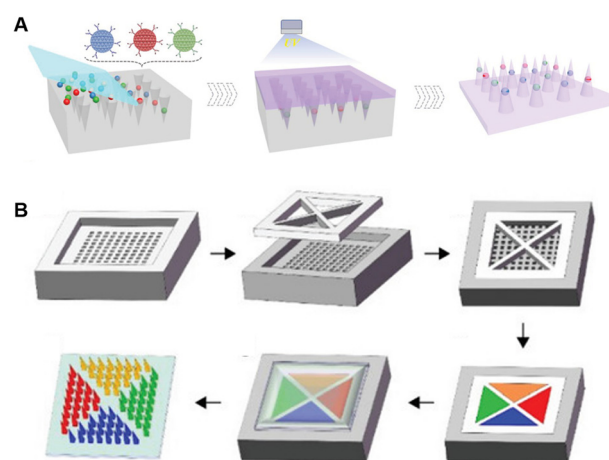
Fig. 4 Schematic illustrations of microneedles for multiplex analysis based on different decoding principles. (A) Color-encoded microneedles loaded with photonic crystals. Reproduced with permission.[115] Copyright 2019, Wiley-VCH Verlag. (B) Tattoo-patterned microneedles for dermal biosensor delivery. Reproduced with permission.[98] Copyright 2021, Wiley-VCH Verlag.

Tehrani *et al.* integrated three sensors in one microneedle device to realize simultaneous real-time sensing of pH, glucose and lactate.[84] Similarly, synchronous detection of ketone bodies, glucose, and lactate is realized within the same strategy.[99] Mishra *et al.* detected fentanyl and organophosphate nerve agents on a single microneedle patch using two different electrode-containing hollow needles.[11] Moreover, the combination of both color- and spatial-differentiation further contributes to a higher throughput. Qiao *et al.* designed different amplification primers to distinguish 11 kinds of psoriasis-related miRNAs. With labelling of cy3, cy5, and FAM, up to three kinds of miRNAs

Table 3 Representative of highly integrated microneedles sensing systems

Principles	Readouts	Targets	Sensing	Microneedle compositions	Detection ranges	Time consumptions/continuous sensing	Ref.
Colorimetric manner	Naked-eye visible	Glucose	GO_x-based TMB-HRP colorimetric systems	PVA-MNs with a PVA colorimetric layer	50–400 mg dL^{-1}	~10 min	120
	Naked-eye visible	Glucose, cholesterol	Oxidase-based MADB/TOPS colorimetric systems	Stainless steel-MNs with a PDMS layer, and two NC membranes	0–270 mg dL^{-1} for glucose, 0–320 mg dL^{-1} for cholesterol	~3 min	125
	Naked-eye visible	*E. coli*, pH	Polydiacetylene liposomal bio-ink binding with antibodies	Silk-MNs	—	<4 h	12
	Naked-eye visible	pH, glucose, uric acid, and temperature	pH indicators, GO_x/uricase-based TMB-HRP colorimetric systems, and temperature responsive solutions	HA-MNs	6.0–8.0 for pH; 1–10 mM for glucose, 0.2–1.6 mM for uric acid, 36–39 °C for temperature	10 min	98
	Naked-eye visible	Glucose, lactate, cholesterol, and pH	Oxidases/HRP/three chromogenic dye systems, and the pH indicator bromocresol green	HA-MeHA-MNs with a NC membrane	0–16 mM for glucose, 0–3.2 mM for lactate, 0–12 mM for cholesterol, 5–8 for pH	10 min	135
	Cellphone-assisted	Glucose	Glucose-responsive colloidal crystal colorimetric systems	Resin-MNs with colloidal crystals	100–400 mg/dL	~5 min	121
	Cellphone-assisted	Uric acid	Uricase/polypyrrole nanoparticles/TMB colorimetric systems	PVA-MNs with a PVA colorimetric layer	200–1000 μM	~40 min	131
Fluorometric manner	Cellphone-assisted with a handheld LED light	DNA	LAMP amplification with nucleic acid dye	PVA-MNs	10–100 ng	30 min	100
	Portable fluorescence reader-assisted	ROS	Redox reaction of PEGylated Cy5	HA-MNs	50–250 μM	20 min	126
Electronic manner	Cellphone-assisted	Glucose	Amperometry	Stainless steel-MNs with PCB electrodes	3–13 mM	Continuous sensing for 21 h	119
	Cellphone- assisted	Glucose, lactate, and alcohol	Chronoamperometry	PMMA-MNs with microelectrodes, an electronic control system, and a Bluetooth package	0.32–40 mM for glucose, 0.15–28 mM for lactate, and 0.50–100 mM for alcohol	<5 min for a single response, and continuous sensing for 12 h	84
	Cellphone- assisted	Tyrosinase	Amperometry, CV	Stainless steel-MNs with a bandage sensor (printing stress-enduring inks)	0.1–0.5 mg mL^{-1}	<2 min	145
	Cellphone- assisted	Glucose	CV	Cyclic olefin copolymer-MNs	0.05–20 mM	Continuous sensing for 72 h	122

could be detected simultaneously at the same tip, and the throughput was further enlarged after the separation of the microneedle bodies.[116]

Comprehensive omics information could also be obtained with the aid of microneedles. Tran *et al.* developed a microneedle array to extract ISF for liquid chromatography mass spectrometry analysis in proteomics. They found that the protein species in ISF were highly similar to those in plasma and serum of the same donors, further supporting the development of ISF biomarkers in the field of *in vitro* diagnosis.[117]

4. Integrated microneedle sensing systems

To meet the demands of point-of-care testing, microneedles have been integrated with other devices to allow direct extraction of biomarkers, rapid detection, and on-site readout. So far, targets of integrated microneedle-integrated detection systems have covered ions,[50,118] small molecules (glucose,[119–122,124] lactate,[30,123] cholesterol[125] and ROS[126,127]), and nucleic acids.[49,100,116,128,129] In this section, we summarize recently reported integrated microneedle sensing devices, highlighting distinct sensing principles including colorimetric, fluorometric and electronic systems (Fig. 1). The modes of data acquisition, recording, and transmission, and the validated models were also included. The representative highly integrated studies mentioned in this section are summarized in Table 3, indicating the targets, detection principles, assay durations, and working ranges.

4.1 Colorimetric systems

Based on the merits of naked eye visibility, easy fabrication and cost effectiveness, colorimetric assays enable qualitative and quantitative analysis, serving a wide range of point-of-care testing (POCT) devices. Relevant data can be directly distinguished with the naked eye, or captured with cellphones, scanners or cameras, and finally analysed through RGB value processing software. Colorimetric systems have been implemented in detections of small molecules (glucose[120,121,130] and uric acid[131]), proteins,[44] and bacteria.[113,132] In general, colorimetric signals are induced by changes in chemical structures, densities, orientations, morphologies, or sizes of chromogenic agents upon interaction with the target substance.[133] Based on different principles of color development, the chromogenic agents could be classified as redox-responsive agents,[120,125,130,134] and nanostructures.[121,135]

In terms of redox-responsive agents, the analytes of interest could be firstly oxidized with a specific oxidase to generate H_2O_2, which could subsequently react with a H_2O_2-responsive chromogenic agent. Paper is a major constituent of these colorimetric assays, owing to its merits of hydrophilicity, portability, and cost effectiveness.[136] For example, Li *et al.*[125] designed a paper-mediated colorimetric

microneedle system to realize dual identification of glucose and cholesterol levels in rabbit models. Glucose and cholesterol were collected *via* a single microneedle, oxidized *via* glucose oxidase (GO_x) and cholesterol oxidase, and finally reacted with *N*-ethyl-*N*-sulfopropyl-*m*-toluidine (TOPS) and *N*,*N*-bis(4-sulfobutyl)-3,5-dimethylaniline disodium salt (MADB) to form purple and green colors, respectively.[125] Similarly, Zeng *et al.* designed paper sensor-integrated microneedles for multi-metabolite analysis in ISF.[134] Moreover, direct addition of chromogenic agents into microneedles enables fully integrated sensor fabrication.[120,121,131,132] Wang *et al.* applied GO_x, horseradish peroxidase (HRP), and 3,3′,5,5′-tetramethylbenzidine (TMB) into PVA layers to realize the *in situ* colorimetric detection of glucose in a type 1 diabetic mouse model. The patch could turn blue on the back side once exposed to a high level of glucose. The color intensity of microneedles could be obtained *via* a miniaturized scanner.[120] Moreover, cellphones have been integrated with colorimetry-based microneedle devices for higher accuracy and sensitivity. Zhang *et al.* described an *in situ* smartphone-assisted microneedle detection of uric acid. Polypyrrole nanoparticles with HRP-like nanoenzyme activities, urease, and TMB were introduced into microneedles, thus producing a blue color in the absence of uric acid. The color intensity was recorded with a cellphone camera, and finally analysed with the MATLAB software.[131]

Introduction of colorimetric nanoparticles is an alternative approach for construction of colorimetric microneedles, such as the widely-used Au nanoparticles (AuNPs). The aggregation of AuNPs could induce color changes from red to blue under the principles of local surface plasmon resonance (LSPR). When the distance between nanoparticles was narrowed, one particle could resonate with neighbours to form new vibrational modes, leading to changes of the absorption
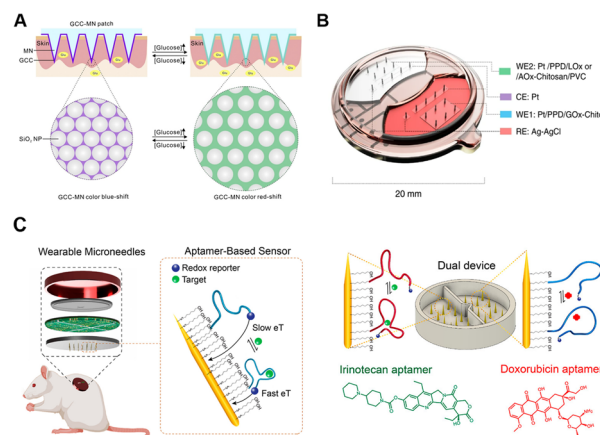
Fig. 5 Schematic diagrams of microneedle-integrated sensing platforms. (A) Colloidal crystal-loaded microneedles for colorimetric detection of glucose. Reproduced with permission.[121] Copyright 2020, Elsevier. (B) Multiplexed microneedle sensor with systematic electronic integration. Reproduced with permission.[84] Copyright 2022, Springer Nature Publishing. (C) Aptamer–based microneedles for electrochemical signal detection. Reproduced with permission.[146] Copyright 2022, American Chemical Society.

spectrum.[135] For example, Puttaswamy *et al.* proposed a combined method of extracting ISF using microneedles, and monitoring cysteine C (Cys C) by a lateral flow immunochromatography assay (LFIA). The sample flow in LFIA was driven by capillary force, and the flowing Cys C and antibody-coated AuNPs were immobilized at a specific position. The Cys C levels were quantified under an immune-sandwich principle, when the AuNPs were aggregated into a naked-eye visible band.[44] Colloidal crystals, a 2D or 3D oriented arrangement of monodisperse particles (*e.g.*, SiO_2 NPs), are featured with photonic band gaps that shift along the array arrangement, thus resulting in macroscopic color changes. Zeng *et al.* modified SiO_2 NP colloidal crystals with glucose-binding fluorophenylboronic acid (FPBA), which was subsequently coated on shells of microneedles. Once in contact, glucose could enter and alter the alignment of FPBA-SiO_2 NPs, resulting in a redshift of the microneedle colors from blue to green (Fig. 5A).[121]

4.2 Fluorometric systems

Fluorescence detection has also been demonstrated to have great potential for sensitive analysis, particularly for proteins[55,115,137] and nucleic acids.[49,100,116,128] Molecules that selectively recognize or interact with targets can be attached to fluorescent labels for an immune sandwich assay, including capturing or detecting antibodies,[115] protein ligands,[138] DNA intercalators,[49] and nucleic acid reporters.[116] For example, Wang *et al.* coated capture antibodies on microneedles for an on-needle fluorophore-linked immunosorbent assay (FLISA). Target proteins were captured by antibodies on the surface of needles, then *ex vivo* treated with secondary antibody-functionalized fluorescent Au nanorods, and finally imaged *via* a fluorescence imager.[137]

Besides direct target recognition, trace analytes like nucleic acids often require signal amplification, such as catalytic hairpin assembly (CHA),[116,128] post-collection polymerase chain reaction (PCR),[8] and loop-mediated isothermal amplification (LAMP).[100] Paul *et al.* designed a microneedle device integrated with a smartphone-based florescence reader and a handheld excited LED light, for detection of pathogen DNA. The microneedles firstly extracted DNA samples by swelling upon insertion into skin, which were then transferred to a reaction chamber to be amplified by LAMP.[100]

Fluorescent tattooing is an emerging sensing technique with higher integration. Microneedles could serve as a medium to deliver the tattoo sensor to the dermis, enabling the construction of a painless *in situ* tattoo sensor. Babity *et al.* loaded hydrocyanines into a dissolvable microneedle array to form a transient ratiometric tattoo, which was non-fluorescent at reduced states, but highly fluorescent in oxidized forms, thus enabling responsive sensing of reactive oxygen species (ROS).[126]

4.3 Electronic systems

Among all the POCT devices, electrochemical systems offer great prospects for commercialization due to the highly integrated and user-friendly virtues for individuals.[139] Meanwhile, the capacities for rapid response, long endurance, high sensitivity and good linearity enable accurate monitoring of trace analytes.[140] Typically, electrochemical systems on microneedles consist of sensors (functionalized for specific target recognition), electronics (for controlling and powering), and wired or wireless data transmitters (Fig. 5B).[84] Electronic analytical techniques are usually flexibly applied to microneedles, such as cyclic voltammetry (CV), differential pulse voltammetry (DPV), square wave voltammetry (SWV), chronoamperometry, and amperometry.[141,142] So far, microneedle-based electronic platforms are mostly applied to detections of ions (pH values,[143] Na^+,[50] and K^+[118]), small molecules (glucose,[30,122,124,144] lactate,[123] and ascorbic acid[139]), nucleic acids,[129] and proteins (cytokines[112,139] and enzymes[145]). For example, tyrosinase (TYR) is a polyphenol oxidase involved in melanin production, whose accumulation leads to the biogenesis of melanoma. Ciui *et al.* designed microneedles for melanoma screening against TYR, functionalized with catechol-coated bandage-shaped electrodes. TYR could oxidize the coated catechol into benzoquinone (BQ), which could be amperometrically quantified at the printed electrodes.[145] To expand the real-time monitoring applications, aptamers were combined with microneedles for specific detection of redox inactive molecules like endotoxins, cocaine, and drugs by reversible affinity interactions.[146,147] Conformationally reversible aptamers were conjugated with redox reporters on microneedles, so that once the aptamers bound with specific targets, the reporters on microneedles alternately moved. Dynamic electron transmission signals can be obtained through distance changes between redox reporters and golden needles (Fig. 5C).[146]

Besides detection sensitivity, selectivity is essential for electrochemical monitoring devices, especially for blood or ISF samples with complex molecular compositions. To address the issues of endogenous interference, which is caused by direct oxidation on electrodes, the microneedles are generally coated or functionalized with enzymes,[148] nano-enzymes,[123] antibodies,[9] polymer layers,[127,129] or permselective membranes.[50] For example, Li *et al.* modified polydopamine nanospheres (PDNS) with AuNPs on Pt microneedles for voltammetric signal detection of lactate. The PDNS served as intermediates between AuNPs and microneedles, enhancing the density of AuNP decoration, and improving the stability of the device.[123] Zheng *et al.* coated a sodium-selective membrane on microneedles for real-time selective monitoring of Na^+. The membrane-functionalized microneedles not only penetrated the skin for sampling, but also accommodated selective electrodes and extended gates, greatly facilitating the construction and integration of a flexible electronic biosensor.[50]

4.4 Device assembly and integration

To meet the growing needs towards high integration and multiple functions, microneedles were assembled with sensing, controlling, and powering components to offer the possibilities of signal conduction, fluidic control, and self-powering. The principles and processes of device integration, especially the electronic components, are discussed below according to different functions.

Integration of a sensing component, which can convert extracted biomarkers into transmitted signals, is of vital significance for expansion of terminal applications. Typically, the sensing component is usually attached to the back of the microneedle array.[53,125,149,150] Once inserted, the extracted biofluid firstly flows out of the back and subsequently enters the detection or sensing zone, and finally, the corresponding outputs are transmitted to mobile phones *via* a wireless transmitter.[50,53] For example, Cheng *et al.* developed a microneedle-based wearable system for long-term glucose monitoring. The sensing component was an electrode coated with GO_x hydrogels, which could produce H_2O_2 and induce electron transfer for detection. By combining a touch activator, a wireless electronic detector and a user-friendly app, a miniaturized and user-friendly electrochemical detection platform was constructed (Fig. 6A).[85] Meanwhile, microbial contamination during long-term wearing poses biosafety challenges for practical applications of the wearable devices. Cost-effective polymeric microneedles provide a disposable choice to balance the biosafety and cost challenges of electronic devices. For example, Lee *et al.* designed a microneedle-based strip-type disposable system to realize glucose monitoring and multistage drug delivery. The polymeric microneedles were assembled with a thermal actuator to allow periodic

replacement.[151] Similarly, Tehrani *et al.* developed a highly-integrated wearable microneedle sensor for multiple biomarker monitoring, including glucose, lactate, and alcohol.[30] Nine distinct subcomponents, including a discardable microneedle array, and reusable electronics, were assembled, enabling convenient replacement of the sampling component.

With the addition of a control component, microneedles are endowed with multiple functions, such as sample handling, and fluidic manipulations. PDMS is widely used to manufacture control components for microneedles, due to the benefits of easy fabrication and flexibility. For example, Li *et al.* constructed a blood-extraction system consisting of a PDMS-fabricated self-recovery actuator and a long hollow microneedle. By integrating an elastic chamber with several valves, the device achieved blood extraction activated by finger pressing.[36] Moreover, the control component could be fabricated by injection-moulding of plastics or rubbers such as acrylonitrile butadiene styrene and thermoplastic elastomers. Blicharz *et al.* assembled a microneedle-based tap-actuated device (named TAP) for painless collection of blood. A solid microneedle array was integrated into the device to withdraw 100 μL blood by a vacuum after skin puncture. The inner microfluidic channel could generate thorough mixing of blood and lithium heparin anticoagulant to achieve blood preservation (Fig. 6B).[15]

Power supply determines the level of integration of certain microneedle systems, especially those combined with electro-osmosis extracting components or electronic sensors. Generally, power is supplied with lithium-ion polymer or coin cell batteries.[30,53] For example, Cheng *et al.* connected a 3.7 V rechargeable lithium coin cell battery to the back of a PCB for power supply.[85] Besides, enzymatic biobatteries can be an alternative for integrating a fully organic disposable transdermal patch. For example, Kusama *et al.* integrated series-connected enzymatic biobatteries (fructose/O_2 battery) for both ISF extraction and drug delivery.[52] Cotton cloth was used as both the reservoir of fructose and the ion conductor in the circuit to drive the transdermal EOF, which demonstrated the feasibility of an entirely organically composited microneedle patch (Fig. 6C).

5. Challenges and perspectives

In this review, we discussed the advances in microneedle-based detection/sensing devices, and the trend towards full integration, digitalization, and intelligent management. Compared to traditional laboratory testing, microneedles offer the merits of minimal invasiveness, rapid readout, patient compliance, miniaturization and high integration, enabling working scopes in community clinics, at-home healthcare, and on-field scenarios. Yet, there is still plenty of room to improve microneedle-based detection/sensing devices to fulfil their great potential in wider applications.

Passive and active extraction of biofluids using microneedles has been established, and the surge in microneedle technology has advanced the field of biofluid
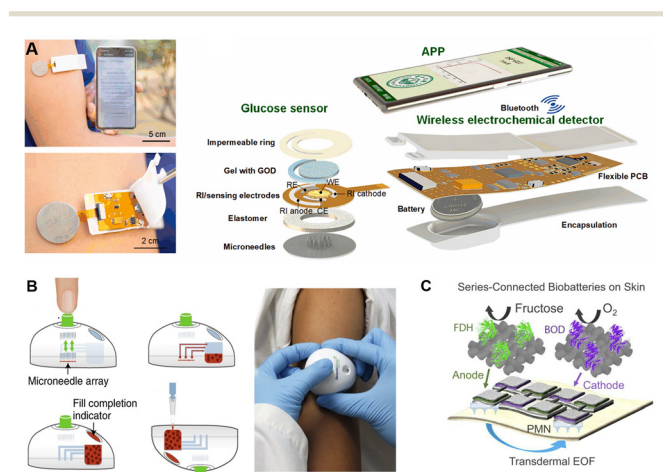
Fig. 6 Schematic illustration of different functional components assembled on microneedles. (A) The assembly of a wireless-transited pattern-integrated glucose sensor. Reproduced with permission.[85] Copyright 2022, Elsevier. (B) Microneedle-based TAP device with inside microfluidic channels for flow control. Reproduced with permission.[15] Copyright 2018, Springer Nature Publishing. (C) A self-powering electronic microneedle array with an enzyme battery. Reproduced with permission.[52] Copyright 2021, Springer Nature Publishing.
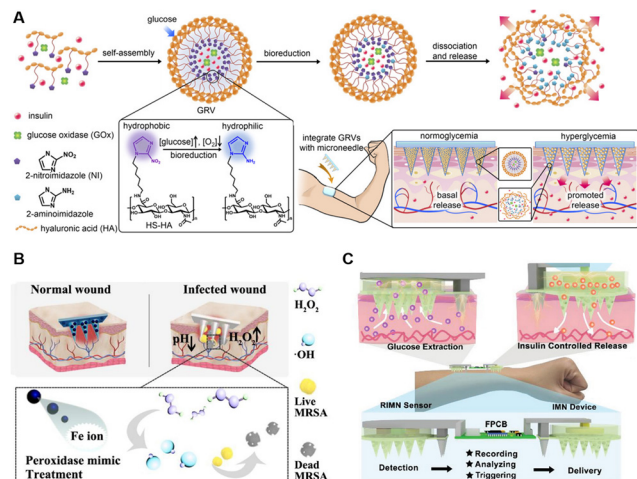
Fig. 7 Schematic illustration of intelligent microneedles integrated with diagnosis and treatment functions. (A) A smart glucose-sensing microneedle patch with hypoxia-responsive vesicles for diabetes treatment. Reproduced with permission.[6] Copyright 2015, National Academy of Sciences. (B) Wound-healing intelligent colorimetric-sensing microneedles. Reproduced with permission.[158] Copyright 2022, Elsevier. (C) Diabetes-treatment electronic-sensing microneedles. Reproduced with permission.[53] Copyright 2021, Wiley-VCH Verlag.

sampling. However, the latency for sub-millilitre ISF draining calls for minutes, whereas a routine phlebotomy could obtain dozens of millilitres. The sampling using microneedle devices needs to be accelerated. Moreover, small analytes in ISF have been partially investigated (Table 1), while the detailed relationship between ISF and blood in abnormal physiological states (in illness or under treatment) still needs to be systematically explored with extensive clinical validations.

Colorimetric, fluorometric, and electronic signal sensing has been integrated to facilitate the construction of microneedle terminal sensors, especially wearable electronic sensors. Recently, several groups have reported the fabrication of electro-microneedles that could work *in vivo* for long periods without interference.[30,53,85] However, the long-term *in vivo* implementation is still an issue in the field concerning calibration and biocompability.[142] Pipelines including biocompatible testings,[152] samplings,[153] and threshold settings[154] still require careful explorations.

The rising theranostic microneedles, combined with both monitoring and treatment functions, initiated an alternative direction for individual healthcare management.[155–157] Yu *et al.* reported a glucose-sensing insulin patch loaded with nanoscale hypoxia-responsive vesicles (Fig. 7A). The encapsulated GO_x could sense the glucose levels, rapidly consume the oxygen under hyperglycemia conditions, and generate a hypoxic environment through enzymatic oxidations, leading to the breaking of vesicles and the release of inside insulin.[6] Moreover, the sensing of glucose by phenylboronic acid and the subsequent responsive release of insulin have also been demonstrated on microneedles.[7] In addition to microneedles cascaded with sensing and releasing functions, theranostic microneedles capable of

outputting signals have also been proposed. Shan *et al.* constructed a wound microenvironment-responsive colorimetric microneedle array for indication of wound conditions as well as the required treatment. The color would change at bacteria-infected sites, while the inside nanozymes could generate ·OH for bacteria killing (Fig. 7B).[158] Moreover, a closed-loop wearable microneedle array has been proposed to sense glucose levels and accordingly treat diabetic mice with insulin (Fig. 7C). The glucose levels could be determined, and wirelessly transited to cellphones. The pre-loaded insulin could be released, triggered by an integrated flexible PCB, revealing impressive capabilities of a smart carry-on personal health care terminal.[53]

In short, as a promising platform, microneedles have been integrated with various detection techniques to realize sampling, sensing, and monitoring capacities. More and more technique crossovers are emerging in conjunction with microneedles to facilitate precise and personalized daily health profiles, such as wireless transitions,[50,84,85,122,145] and digital recording.[65,159] Further advances in microneedle-based devices could be expected with novel biomarker discovery in ISF, *in vivo* biocompatibility and stability improvements, and theranostic health management.

Author contributions

Supervision: Z. G. and Y. Z. Writing – original draft: J. W., Z. L., R. C., and H. Z. Writing – review & editing: Z. G., Y. Z., and J. Y.

Conflicts of interest

Z. G. is the co-founder of Zenomics Inc., ZCapsule Inc., and μZen Pharm Co., Ltd., and the other authors declare no conflict of interest.

Acknowledgements

Notes and references

1 M. Janssen, J. Scheerder, E. Thibaut, A. Brombacher and S. Vos, *PLoS One*, 2017, **12**, e0181167.
2 J. McLenon and M. A. M. Rogers, *J. Adv. Nurs.*, 2019, **75**, 30–42.
3 S. Hashmi, P. Ling, G. Hashmi, M. Reed, R. Gaugler and W. Trimmer, *BioTechniques*, 1995, **19**, 766–770.
4 S. Henry, D. V. McAllister, M. G. Allen and M. R. Prausnitz, *J. Pharm. Sci.*, 1998, **87**, 922–925.

5 W. H. Smart and K. Subramanian, *Diabetes Technol. Ther.*, 2000, **2**, 549–559.

6 J. Yu, Y. Zhang, Y. Ye, R. DiSanto, W. Sun, D. Ranson, F. S. Ligler, J. B. Buse and Z. Gu, *Proc. Natl. Acad. Sci. U. S. A.*, 2015, **112**, 8260–8265.

7 J. Yu, J. Wang, Y. Zhang, G. Chen, W. Mao, Y. Ye, A. R. Kahkoska, J. B. Buse, R. Langer and Z. Gu, *Nat. Biomed. Eng.*, 2020, **4**, 499–506.

8 H. Becker, B. L. Gray, T. Minogue, J. Duy, S. Collins and R. Smith, *presented in part at the Microfluidics, BioMEMS, and Medical Microsystems XVI*, 2018.

9 M. Dervisevic, M. Alba, T. E. Adams, B. Prieto-Simon and N. H. Voelcker, *Biosens. Bioelectron.*, 2021, **192**, 113496.

10 R. Paul, A. C. Saville, J. C. Hansel, Y. Ye, C. Ball, A. Williams, X. Chang, G. Chen, Z. Gu, J. B. Ristaino and Q. Wei, *ACS Nano*, 2019, **13**, 6540–6549.

11 R. K. Mishra, K. Y. Goud, Z. Li, C. Moonla, M. A. Mohamed, F. Tehrani, H. Teymourian and J. Wang, *J. Am. Chem. Soc.*, 2020, **142**, 5991–5995.

12 D. Kim, Y. Cao, D. Mariappan, M. S. Bono Jr, A. J. Hart and B. Marelli, *Adv. Funct. Mater.*, 2021, **31**, 2005370.

13 A. Catala, R. Culp-Hill, T. Nemkov and A. D'Alessandro, *Metabolomics*, 2018, **14**, 100.

14 J. Xing, J. Loureiro, M. T. Patel, D. Mikhailov and A. I. Gusev, *Bioanalysis*, 2020, **12**, 919–935.

15 T. M. Blicharz, P. Gong, B. M. Bunner, L. L. Chu, K. M. Leonard, J. A. Wakefield, R. E. Williams, M. Dadgar, C. A. Tagliabue, R. El Khaja, S. L. Marlin, R. Haghgooie, S. P. Davis, D. E. Chickering and H. Bernstein, *Nat. Biomed. Eng.*, 2018, **2**, 151–157.

16 P. E. Laurent, S. Bonnet, P. Alchas, P. Regolini, J. A. Mikszta, R. Pettis and N. G. Harvey, *Vaccine*, 2007, **25**, 8833–8842.

17 R. L. Atmar, S. M. Patel and W. A. Keitel, *Expert Rev. Vaccines*, 2010, **9**, 1399–1409.

18 P. Van Damme, F. Oosterhuis-Kafeja, M. Van der Wielen, Y. Almagor, O. Sharon and Y. Levin, *Vaccine*, 2009, **27**, 454–459.

19 P. Xue, L. Zhang, Z. Xu, J. Yan, Z. Gu and Y. Kang, *Appl. Mater. Today*, 2018, **13**, 144–157.

20 X. Liu, J. Cleary and G. K. German, *Acta Biomater.*, 2016, **43**, 78–87.

21 Y. Yuan and R. Verma, *Colloids Surf., B*, 2006, **48**, 6–12.

22 M. A. Kendall, Y. F. Chong and A. Cock, *Biomaterials*, 2007, **28**, 4968–4977.

23 X. Feng, G.-Y. Li, A. Ramier, A. M. Eltony and S.-H. Yun, *Acta Biomater.*, 2022, **146**, 295–305.

24 G. Cevc and U. Vierl, *J. Controlled Release*, 2007, **118**, 18–26.

25 J. N. Roe and B. R. Smoller, *Crit. Rev. Ther. Drug Carrier Syst.*, 1998, **15**, 199–241.

26 J. Heikenfeld, A. Jajack, B. Feldman, S. W. Granger, S. Gaitonde, G. Begtrup and B. A. Katchman, *Nat. Biotechnol.*, 2019, **37**, 407–419.

27 N. Fogh-Andersen, B. M. Altura, B. T. Altura and O. Siggaard-Andersen, *Clin. Chem.*, 1995, **41**, 1522–1525.

28 F. J. Service, P. C. O'Brien, S. D. Wise, S. Ness and S. M. LeBlanc, *Diabetes Care*, 1997, **20**, 1426–1429.

29 S. Mitragotri, M. Coleman, J. Kost and R. Langer, *Pharm. Res.*, 2000, **17**, 466–470.

30 F. Tehrani, H. Teymourian, B. Wuerstle, J. Kavner, R. Patel, A. Furmidge, R. Aghavali, H. Hosseini-Toudeshki, C. Brown, F. Zhang, K. Mahato, Z. Li, A. Barfidokht, L. Yin, P. Warren, N. Huang, Z. Patel, P. P. Mercier and J. Wang, *Nat. Biomed. Eng.*, 2022, **6**(11), 1214–1224.

31 P. P. Samant, M. M. Niedzwiecki, N. Raviele, V. Tran, J. Mena-Lapaix, D. I. Walker, E. I. Felner, D. P. Jones, G. W. Miller and M. R. Prausnitz, *Sci. Transl. Med.*, 2020, **12**(571), eaaw0285.

32 J. Cohen, R. Deans, A. Dalley, J. Lipman, M. S. Roberts and B. Venkatesh, *J. Crit. Care*, 2009, **13**, R189.

33 I. M. Cooke, R. P. Bevill, D. R. Nelson and G. D. Koritz, *Vet. Res.*, 1996, **27**, 147–159.

34 J. Zhu, X. Zhou, H. J. Kim, M. Qu, X. Jiang, K. Lee, L. Ren, Q. Wu, C. Wang, X. Zhu, P. Tebon, S. Zhang, J. Lee, N. Ashammakhi, S. Ahadian, M. R. Dokmeci, Z. Gu, W. Sun and A. Khademhosseini, *Small*, 2020, **16**, e1905910.

35 C. G. Li, M. Dangol, C. Y. Lee, M. Jang and H. Jung, *Lab Chip*, 2015, **15**, 382–390.

36 C. G. Li, K. Lee, C. Y. Lee, M. Dangol and H. Jung, *Adv. Mater.*, 2012, **24**, 4583–4586.

37 L. M. Strambini, A. Longo, A. Diligenti and G. Barillaro, *Lab Chip*, 2012, **12**, 3370–3379.

38 K. Tsuchiya, N. Nakanishi, Y. Uetsuji and E. Nakamachi, *Biomed. Microdevices*, 2005, **7**, 347–353.

39 Y. Li, H. Zhang, R. Yang, Y. Laffitte, U. Schmill, W. Hu, M. Kaddoura, E. J. M. Blondeel and B. Cui, *Microsyst. Nanoeng.*, 2019, **5**, 41.

40 P. R. Miller, R. M. Taylor, B. Q. Tran, G. Boyd, T. Glaros, V. H. Chavez, R. Krishnakumar, A. Sinha, K. Poorey, K. P. Williams, S. S. Branda, J. T. Baca and R. Polsky, *Commun. Biol.*, 2018, **1**, 173.

41 J. R. Windmiller, N. Zhou, M. C. Chuang, G. Valdés-Ramírez, P. Santhosh, P. R. Miller, R. Narayan and J. Wang, *Analyst*, 2011, **136**, 1846–1851.

42 E. V. Mukerjee, S. D. Collins, R. R. Isseroff and R. L. Smith, *Sens. Actuators, A*, 2004, **114**, 267–275.

43 E. M. Cahill, S. Keaveney, V. Stuettgen, P. Eberts, P. Ramos-Luna, N. Zhang, M. Dangol and E. D. O'Cearbhaill, *Acta Biomater.*, 2018, **80**, 401–411.

44 S. V. Puttaswamy, G. V. Lubarsky, C. Kelsey, X. Zhang, D. Finlay, J. A. McLaughlin and N. Bhalla, *ACS Nano*, 2020, **14**, 11939–11949.

45 S. Jiang, P. Li, Y. Yu, J. Liu and Z. Yang, *J. Biomech.*, 2014, **47**, 3344–3353.

46 P. P. Samant and M. R. Prausnitz, *Proc. Natl. Acad. Sci. U. S. A.*, 2018, **115**, 4583–4588.

47 R. He, Y. Niu, Z. Li, A. Li, H. Yang, F. Xu and F. Li, *Adv. Healthcare Mater.*, 2020, **9**, e1901201.

48 A. Mandal, A. V. Boopathy, L. K. W. Lam, K. D. Moynihan, M. E. Welch, N. R. Bennett, M. E. Turvey, N. Thai, J. H. Van, J. C. Love, P. T. Hammond and D. J. Irvine, *Sci. Transl. Med.*, 2018, **10**(467), eaar2227.

49 D. Al Sulaiman, J. Y. H. Chang, N. R. Bennett, H. Topouzi, C. A. Higgins, D. J. Irvine and S. Ladame, *ACS Nano*, 2019, **13**, 9620–9628.

50 Y. Zheng, R. Omar, R. Zhang, N. Tang, M. Khatib, Q. Xu, Y. Milyutin, W. Saliba, Y. Y. Broza, W. Wu, M. Yuan and H. Haick, *Adv. Mater.*, 2022, **34**, e2108607.

51 H. Chang, M. Zheng, X. Yu, A. Than, R. Z. Seeni, R. Kang, J. Tian, D. P. Khanh, L. Liu, P. Chen and C. Xu, *Adv. Mater.*, 2017, **29**, 1702243.

52 S. Kusama, K. Sato, Y. Matsui, N. Kimura, H. Abe, S. Yoshida and M. Nishizawa, *Nat. Commun.*, 2021, **12**, 658.

53 X. Li, X. Huang, J. Mo, H. Wang, Q. Huang, C. Yang, T. Zhang, H. J. Chen, T. Hang, F. Liu, L. Jiang, Q. Wu, H. Li, N. Hu and X. Xie, *Adv. Sci.*, 2021, **8**, e2100827.

54 Y. E. Kang, K. Y. Seong, S. G. Yim, Y. Lee, S. M. An, S. C. Kim, K. Kim, B. S. An, K. S. Lee and S. Y. Yang, *Biosens. Bioelectron.*, 2020, **163**, 112281.

55 K. Yi, Y. Wang, K. Shi, J. Chi, J. Lyu and Y. Zhao, *Biosens. Bioelectron.*, 2021, **190**, 113404.

56 Z. Wang, J. Luan, A. Seth, L. Liu, M. You, P. Gupta, P. Rathi, Y. Wang, S. Cao, Q. Jiang, X. Zhang, R. Gupta, Q. Zhou, J. J. Morrissey, E. L. Scheller, J. S. Rudra and S. Singamaneni, *Nat. Biomed. Eng.*, 2021, **5**, 64–76.

57 W. Chen, Z. Wang, L. Wang and X. Chen, *Adv. Mater.*, 2022, **34**, e2106701.

58 J. L. Tan, J. Tien, D. M. Pirone, D. S. Gray, K. Bhadriraju and C. S. Chen, *Proc. Natl. Acad. Sci. U. S. A.*, 2003, **100**, 1484–1489.

59 B. Gonenc, R. H. Taylor, I. Iordachita, P. Gehlbach and J. Handa, *Proc. IEEE Sens.*, 2014, **2014**, 698–701.

60 T. Zhang, B. Chen and S. Zuo, *IEEE Trans. Ind. Electron.*, 2022, **69**, 940–949.

61 B. L. Zhang, X. P. Zhang, B. Z. Chen, W. M. Fei, Y. Cui and X. D. Guo, *Microchem. J.*, 2021, **162**, 105830.

62 M. Kim, T. Kim, D. S. Kim and W. K. Chung, *Sensors*, 2015, **15**, 16265–16280.

63 G. S. Guvanasen, L. Guo, R. J. Aguilar, A. L. Cheek, C. S. Shafor, S. Rajaraman, T. R. Nichols and S. P. DeWeerth, *IEEE Trans. Neural Syst. Rehabilitation Eng.*, 2017, **25**, 1440–1452.

64 R. Wang, J. Bai, X. Zhu, Z. Li, L. Cheng, G. Zhang and W. Zhang, *Biomed. Microdevices*, 2022, **24**, 27.

65 A. K. Srivastava, B. Bhartia, K. Mukhopadhyay and A. Sharma, *Sens. Actuators, A*, 2015, **236**, 164–172.

66 L.-F. Wang, J.-Q. Liu, X.-X. Yan, B. Yang and C.-S. Yang, *Microsyst. Technol.*, 2013, **19**, 269–276.

67 P. R. Miller, X. Xiao, I. Brener, D. B. Burckel, R. Narayan and R. Polsky, *Adv. Healthcare Mater.*, 2014, **3**, 876–881.

68 H. Teymourian, F. Tehrani, K. Mahato and J. Wang, *Adv. Healthcare Mater.*, 2021, **10**, 2002255.

69 H. Li, G. Wu, Z. Weng, H. Sun, R. Nistala and Y. Zhang, *ACS Sens.*, 2021, **6**, 2181–2190.

70 P. R. Miller, S. A. Skoog, T. L. Edwards, D. M. Lopez, D. R. Wheeler, D. C. Arango, X. Xiao, S. M. Brozik, J. Wang, R. Polsky and R. J. Narayan, *Talanta*, 2012, **88**, 739–742.

71 W. Lee, S.-h. Jeong, Y.-W. Lim, H. Lee, J. Kang, H. Lee, I. Lee, H.-S. Han, S. Kobayashi, M. Tanaka and B.-S. Bae, *Sci. Adv.*, 2021, **7**(48), eabi6290.

72 G. K. Mani, K. Miyakoda, A. Saito, Y. Yasoda, K. Kajiwara, M. Kimura and K. Tsuchiya, *ACS Appl. Mater. Interfaces*, 2017, **9**, 21651–21659.

73 J. E. Park, N. Yonet-Tanyeri, E. Vander Ende, A.-I. Henry, B. E. Perez White, M. Mrksich and R. P. Van Duyne, *Nano Lett.*, 2019, **19**, 6862–6868.

74 C. Pan, X. Li, J. Sun, Z. Li, L. Zhang, W. Qian, P. Wang and J. Dong, *ACS Appl. Bio Mater.*, 2019, **2**, 2102–2108.

75 Z. Li, C. Pan, J. Sun, W. Qian and J. Dong, *ACS Food Sci. Technol.*, 2021, **1**, 1787–1791.

76 D. K. Ming, S. Jangam, S. A. N. Gowers, R. Wilson, D. M. E. Freeman, M. G. Boutelle, A. E. G. Cass, D. O'Hare and A. H. Holmes, *BMJ Innov.*, 2022, **8**, 87.

77 P. Bollella, S. Sharma, A. E. G. Cass and R. Antiochia, *Biosens. Bioelectron.*, 2019, **123**, 152–159.

78 Q. Li, Y. Zhang, H. Fan, Y. Gong, Y. Xu, Q. Lv, Y. Xu, F. Xiao, S. Wang, Z. Wang and L. Wang, *Biosens. Bioelectron.*, 2021, **191**, 113474.

79 A. El-Laboudi, N. S. Oliver, A. Cass and D. Johnston, *Diabetes Technol. Ther.*, 2012, **15**, 101–115.

80 D. Bruen, C. Delaney, L. Florea and D. Diamond, *Sensors*, 2017, **17**(8), 1866.

81 J. Ju, L. Li, S. Regmi, X. Zhang and S. Tang, *Biosensors*, 2022, **12**(8), 606.

82 I. D. Federation, *IDF Diabetes Atlas*, 10th edn, 2021, https://www.idf.org/.

83 T. Battelino, M. Phillip, N. Bratina, R. Nimri, P. Oskarsson and J. Bolinder, *Diabetes Care*, 2011, **34**, 795–800.

84 F. Tehrani, H. Teymourian, B. Wuerstle, J. Kavner, R. Patel, A. Furmidge, R. Aghavali, H. Hosseini-Toudeshki, C. Brown, F. Zhang, K. Mahato, Z. Li, A. Barfidokht, L. Yin, P. Warren, N. Huang, Z. Patel, P. P. Mercier and J. Wang, *Nat. Biomed. Eng.*, 2022, **6**(11), 1214–1224.

85 Y. Cheng, X. Gong, J. Yang, G. Zheng, Y. Zheng, Y. Li, Y. Xu, G. Nie, X. Xie, M. Chen, C. Yi and L. Jiang, *Biosens. Bioelectron.*, 2022, **203**, 114026.

86 H. Lee, T. K. Choi, Y. B. Lee, H. R. Cho, R. Ghaffari, L. Wang, H. J. Choi, T. D. Chung, N. Lu, T. Hyeon, S. H. Choi and D.-H. Kim, *Nat. Nanotechnol.*, 2016, **11**, 566–572.

87 S. A. Ranamukhaarachchi, C. Padeste, M. Dübner, U. O. Häfeli, B. Stoeber and V. J. Cadarso, *Sci. Rep.*, 2016, **6**, 29075.

88 T. M. Rawson, S. A. N. Gowers, D. M. E. Freeman, R. C. Wilson, S. Sharma, M. Gilchrist, A. MacGowan, A. Lovering, M. Bayliss, M. Kyriakides, P. Georgiou, A. E. G. Cass, D. O'Hare and A. H. Holmes, *Lancet Digital Health*, 2019, **1**, e335–e343.

89 P. Joshi, P. R. Riley, R. Mishra, S. Azizi Machekposhti and R. Narayan, *Biosensors*, 2022, **12**(4), 198.

90 K. Y. Goud, K. Mahato, H. Teymourian, K. Longardner, I. Litvan and J. Wang, *Sens. Actuators, B*, 2022, **354**, 131234.

91 K. Y. Goud, C. Moonla, R. K. Mishra, C. Yu, R. Narayan, I. Litvan and J. Wang, *ACS Sens.*, 2019, **4**, 2196–2204.

92   D. Nutt, A. Hayes, L. Fonville, R. Zafar, E. O. C. Palmer, L. Paterson and A. Lingford-Hughes, *Nutrients*, 2021, **13**(11), 3938.

93   A. M. V. Mohan, J. R. Windmiller, R. K. Mishra and J. Wang, *Biosens. Bioelectron.*, 2017, **91**, 574–579.

94   T. Wang, H. Zhu, J. Zhuo, Z. Zhu, P. Papakonstantinou, G. Lubarsky, J. Lin and M. Li, *Anal. Chem.*, 2013, **85**, 10289–10295.

95   Q. Jin, H.-J. Chen, X. Li, X. Huang, Q. Wu, G. He, T. Hang, C. Yang, Z. Jiang, E. Li, A. Zhang, Z. Lin, F. Liu and X. Xie, *Small*, 2019, **15**, 1804298.

96   C. Giordano, O. Karasik, K. King-Morris and A. Asmar, *Dis. Markers*, 2015, **2015**, 382918.

97   D. F. S. Fonseca, P. C. Costa, I. F. Almeida, P. Dias-Pereira, I. Correia-Sá, V. Bastos, H. Oliveira, C. Vilela, A. J. D. Silvestre and C. S. R. Freire, *Macromol. Biosci.*, 2020, **20**, 2000195.

98   R. He, H. Liu, T. Fang, Y. Niu, H. Zhang, F. Han, B. Gao, F. Li and F. Xu, *Adv. Sci.*, 2021, **8**, e2103030.

99   H. Teymourian, C. Moonla, F. Tehrani, E. Vargas, R. Aghavali, A. Barfidokht, T. Tangkuaram, P. P. Mercier, E. Dassau and J. Wang, *Anal. Chem.*, 2020, **92**, 2291–2300.

100 R. Paul, E. Ostermann, Y. Chen, A. C. Saville, Y. Yang, Z. Gu, A. E. Whitfield, J. B. Ristaino and Q. Wei, *Biosens. Bioelectron.*, 2021, **187**, 113312.

101 L. S. Young and A. B. Rickinson, *Nat. Rev. Cancer*, 2004, **4**, 757–768.

102 B. Yang, X. Fang and J. Kong, *ACS Appl. Mater. Interfaces*, 2019, **11**, 38448–38458.

103 B. Yang, X. Fang and J. Kong, *Adv. Funct. Mater.*, 2020, **30**, 2000591.

104 B. Yang, J. Kong and X. Fang, *Nat. Commun.*, 2022, **13**, 3999.

105 H. Li, J. Feng, Y. Wang, G. Liu, X. Chen and L. Fu, *J. Agric. Food Chem.*, 2021, **69**, 6879–6887.

106 N. Rifai, M. A. Gillette and S. A. Carr, *Nat. Biotechnol.*, 2006, **24**, 971–983.

107 S. Aydin, K. Ugur, S. Aydin, İ. Sahin and M. Yardim, *Vasc. Health Risk Manage.*, 2019, **15**, 1–10.

108 P. Miller, M. Moorman, R. Manginell, C. Ashlee, I. Brener, D. Wheeler, R. Narayan and R. Polsky, *Electroanalysis*, 2016, **28**, 1305–1310.

109 M. G. Shlipak, M. D. Mattes and C. A. Peralta, *Am. J. Kidney Dis.*, 2013, **62**, 595–603.

110 L. Chen, C. Zhang, J. Xiao, J. You, W. Zhang, Y. Liu, L. Xu, A. Liu, H. Xin and X. Wang, *Mater. Sci. Eng., C*, 2020, **109**, 110402.

111 M. Wang, X. Zhai, J. Li, J. Guan, S. Xu, Y. Li and H. Zhu, *Front. Immunol.*, 2021, **12**, 670391.

112 N. Song, P. Xie, W. Shen, H. Oh, Y. Zhang, F. Vitale, M. Javanmard and M. G. Allen, *Microsyst. Nanoeng.*, 2021, **7**, 96.

113 Y. Wang, H. Ni, H. Li, J. Chen, D. Zhang and L. Fu, *Chem. Eng. J.*, 2022, **442**, 136140.

114 A. Mandal, A. V. Boopathy, L. K. W. Lam, K. D. Moynihan, M. E. Welch, N. R. Bennett, M. E. Turvey, N. Thai, J. H. Van, J. C. Love, P. T. Hammond and D. J. Irvine, *Sci. Transl. Med.*, 2018, **10**, eaar2227.

115 X. Zhang, G. Chen, F. Bian, L. Cai and Y. Zhao, *Adv. Mater.*, 2019, **31**, e1902825.

116 Y. Qiao, J. Du, R. Ge, H. Lu, C. Wu, J. Li, S. Yang, S. Zada, H. Dong and X. Zhang, *Anal. Chem.*, 2022, **94**, 5538–5545.

117 B. Q. Tran, P. R. Miller, R. M. Taylor, G. Boyd, P. M. Mach, C. N. Rosenzweig, J. T. Baca, R. Polsky and T. Glaros, *J. Proteome Res.*, 2018, **17**, 479–485.

118 M. Parrilla, M. Cuartero, S. Padrell Sanchez, M. Rajabi, N. Roxhed, F. Niklaus and G. A. Crespo, *Anal. Chem.*, 2019, **91**, 1578–1586.

119 Y. Cheng, X. Gong, J. Yang, G. Zheng, Y. Zheng, Y. Li, Y. Xu, G. Nie, X. Xie, M. Chen, C. Yi and L. Jiang, *Biosens. Bioelectron.*, 2022, **203**, 114026.

120 Z. Wang, H. Li, J. Wang, Z. Chen, G. Chen, D. Wen, A. Chan and Z. Gu, *Biomaterials*, 2020, **237**, 119782.

121 Y. Zeng, J. Wang, Z. Wang, G. Chen, J. Yu, S. Li, Q. Li, H. Li, D. Wen, Z. Gu and Z. Gu, *Nano Today*, 2020, **35**, 100984.

122 K. B. Kim, W.-C. Lee, C.-H. Cho, D.-S. Park, S. J. Cho and Y.-B. Shim, *Sens. Actuators, B*, 2019, **281**, 14–21.

123 Q. Li, Y. Zhang, H. Fan, Y. Gong, Y. Xu, Q. Lv, Y. Xu, F. Xiao, S. Wang, Z. Wang and L. Wang, *Biosens. Bioelectron.*, 2021, **191**, 113474.

124 O. Heifler, E. Borberg, N. Harpak, M. Zverzhinetsky, V. Krivitsky, I. Gabriel, V. Fourman, D. Sherman and F. Patolsky, *ACS Nano*, 2021, **15**, 12019–12033.

125 C. G. Li, H. A. Joung, H. Noh, M. B. Song, M. G. Kim and H. Jung, *Lab Chip*, 2015, **15**, 3286–3292.

126 S. Babity, F. Couture, E. V. R. Campos, S. Hedtrich, R. Hagen, D. Fehr, M. Bonmarin and D. Brambilla, *Adv. Healthcare Mater.*, 2022, **11**, e2102070.

127 Q. Jin, H. J. Chen, X. Li, X. Huang, Q. Wu, G. He, T. Hang, C. Yang, Z. Jiang, E. Li, A. Zhang, Z. Lin, F. Liu and X. Xie, *Small*, 2019, **15**, e1804298.

128 J. Li, H. Lu, Y. Wang, S. Yang, Y. Zhang, W. Wei, Y. Qiao, W. Dai, R. Ge and H. Dong, *Anal. Chem.*, 2022, **94**, 968–974.

129 B. Yang, X. Fang and J. Kong, *Adv. Funct. Mater.*, 2020, **30**, 2000591.

130 D. Nicholas, K. A. Logan, Y. Sheng, J. Gao, S. Farrell, D. Dixon, B. Callan, A. P. McHale and J. F. Callan, *Int. J. Pharm.*, 2018, **547**, 244–249.

131 P. Zhang, X. Wu, H. Xue, Y. Wang, X. Luo and L. Wang, *Anal. Chim. Acta*, 2022, **1212**, 339911.

132 D. Kim, Y. Cao, D. Mariappan, M. S. Bono, A. J. Hart and B. Marelli, *Adv. Funct. Mater.*, 2020, **31**, 2005370.

133 E. Mauriz, *Sensors*, 2020, **20**, 6214.

134 D. D. Zhu, L. W. Zheng, P. K. Duong, R. H. Cheah, X. Y. Liu, J. R. Wong, W. J. Wang, S. T. Tien Guan, X. T. Zheng and P. Chen, *Biosens. Bioelectron.*, 2022, **212**, 114412.

135 J. Zeng, Y. Zhang, T. Zeng, R. Aleisa, Z. Qiu, Y. Chen, J. Huang, D. Wang, Z. Yan and Y. Yin, *Nano Today*, 2020, **32**, 100855.

136 Y.-Q. Li and L. Feng, *Chin. J. Anal. Chem.*, 2020, **48**, 1448–1457.

137 Z. Wang, J. Luan, A. Seth, L. Liu, M. You, P. Gupta, P. Rathi, Y. Wang, S. Cao, Q. Jiang, X. Zhang, R. Gupta, Q. Zhou, J. J. Morrissey, E. L. Scheller, J. S. Rudra and S. Singamaneni, *Nat. Biomed. Eng.*, 2021, **5**, 64–76.

138 X. Dong, B. Ma, L. Lei, Y. Chen, C. Xu, C. Zhao and H. Liu, *Chem. Eng. J.*, 2022, **432**, 134234.

139 E. Skaria, B. A. Patel, M. S. Flint and K. W. Ng, *Anal. Chem.*, 2019, **91**, 4436–4443.

140 L. Fang, H. Ren, X. Mao, S. Zhang, Y. Cai, S. Xu, Y. Zhang, L. Li, X. Ye and B. Liang, *Biosensors*, 2022, **12**, 102.

141 Q. Wang, X. Wen and J. Kong, *Crit. Rev. Anal. Chem.*, 2020, **50**, 359–375.

142 J. J. García-Guzmán, C. Pérez-Ràfols, M. Cuartero and G. A. Crespo, *TrAC, Trends Anal. Chem.*, 2021, **135**, 116148.

143 S. R. Chinnadayyala, I. Park and S. Cho, *Microchim. Acta*, 2018, **185**, 250.

144 Y. Liu, Q. Yu, X. Luo, L. Yang and Y. Cui, *Microsyst. Nanoeng.*, 2021, **7**, 75.

145 B. Ciui, A. Martin, R. K. Mishra, B. Brunetti, T. Nakagawa, T. J. Dawkins, M. Lyu, C. Cristea, R. Sandulescu and J. Wang, *Adv. Healthcare Mater.*, 2018, **7**, e1701264.

146 Y. Wu, F. Tehrani, H. Teymourian, J. Mack, A. Shaver, M. Reynoso, J. Kavner, N. Huang, A. Furmidge, A. Duvvuri, Y. Nie, L. M. Laffel, F. J. Doyle, 3rd, M. E. Patti, E. Dassau, J. Wang and N. Arroyo-Curras, *Anal. Chem.*, 2022, **94**, 8335–8345.

147 Y. Wu, I. Belmonte, K. S. Sykes, Y. Xiao and R. J. White, *Anal. Chem.*, 2019, **91**, 15335–15344.

148 R. K. Mishra, A. M. Vinu Mohan, F. Soto, R. Chrostowski and J. Wang, *Analyst*, 2017, **142**, 918–924.

149 L. M. Strambini, A. Longo, S. Scarano, T. Prescimone, I. Palchetti, M. Minunni, D. Giannessi and G. Barillaro, *Biosens. Bioelectron.*, 2015, **66**, 162–168.

150 P. R. Miller, X. Xiao, I. Brener, D. B. Burckel, R. Narayan and R. Polsky, *Adv. Healthcare Mater.*, 2014, **3**, 876–881.

151 H. Lee, C. Song, Y. S. Hong, M. Kim, H. R. Cho, T. Kang, K. Shin, S. H. Choi, T. Hyeon and D.-H. Kim, *Sci. Adv.*, 2017, **3**, e1601314.

152 D. Chen, C. Wang, W. Chen, Y. Chen and J. X. Zhang, *Biosens. Bioelectron.*, 2015, **74**, 1047–1052.

153 S. Sharma, A. El-Laboudi, M. Reddy, N. Jugnee, S. Sivasubramaniyam, M. El Sharkawy, P. Georgiou, D. Johnston, N. Oliver and A. E. G. Cass, *Anal. Methods*, 2018, **10**, 2088–2095.

154 N. Vasylieva, S. Marinesco, D. Barbier and A. Sabac, *Biosens. Bioelectron.*, 2015, **72**, 148–155.

155 J. Yu, Y. Zhang, J. Yan, A. R. Kahkoska and Z. Gu, *Int. J. Pharm.*, 2018, **544**, 350–357.

156 P. Makvandi, R. Jamaledin, G. Chen, Z. Baghbantaraghdari, E. N. Zare, C. Di Natale, V. Onesto, R. Vecchione, J. Lee, F. R. Tay, P. Netti, V. Mattoli, A. Jaklenec, Z. Gu and R. Langer, *Mater. Today*, 2021, **47**, 206–222.

157 Y. Lu, A. A. Aimetti, R. Langer and Z. Gu, *Nat. Rev. Mater.*, 2016, **2**, 16075.

158 J. Shan, X. Zhang, B. Kong, Y. Zhu, Z. Gu, L. Ren and Y. Zhao, *Chem. Eng. J.*, 2022, **444**, 136640.

159 L. Ren, Z. Chen, H. Wang, Z. Dou, B. Liu and L. Jiang, *IEEE Trans. Instrum. Meas.*, 2020, **69**, 8328–8334.